Science of the Total Environment 624 (2018) 1523–1538

Contents lists available at ScienceDirect

Science of the Total Environment

journal homepage: www.elsevier.com/locate/scitotenv

Spatial and temporal characteristics of droughts in Central Asia during 1966–2015

Hao Guo [a,b,c,d,g], Anming Bao [a,d,g,*], Tie Liu [a,d,g], Guli·Jiapaer [a], Felix Ndayisaba [e,f], Liangliang Jiang [a,b,c,d,g], Alishir Kurban [a,d,g], Philippe De Maeyer [c,d,g]

[a] State Key Laboratory of Desert and Oasis Ecology, Xinjiang Institute of Ecology and Geography, Chinese Academy of Sciences, Urumqi 830011, China
[b] University of Chinese Academy of Sciences, Beijing 100039, China
[c] Department of Geography, Ghent University, Ghent 9000, Belgium
[d] Sino-Belgian Joint Laboratory of Geo-information, Urumqi, China
[e] Institute of Remote Sensing and Digital Earth, Chinese Academy of Sciences, Beijing 100094, China
[f] Faculty of Environmental Sciences, University of Lay Adventists of Kigali (UNILAK), P.O. 6392, Kigali, Rwanda
[g] Sino-Belgian Joint Laboratory of Geo-information, Ghent, Belgium

HIGHLIGHTS

- Six sub-regions with distinct drought behaviors are identified.
- The spatiotemporal characteristics of retrospective droughts are analyzed.
- An overall wetting trend with a drying switch since 2003 is detected.
- The drought variation is mainly dominated by the periodicity of 16–64 months.

GRAPHICAL ABSTRACT

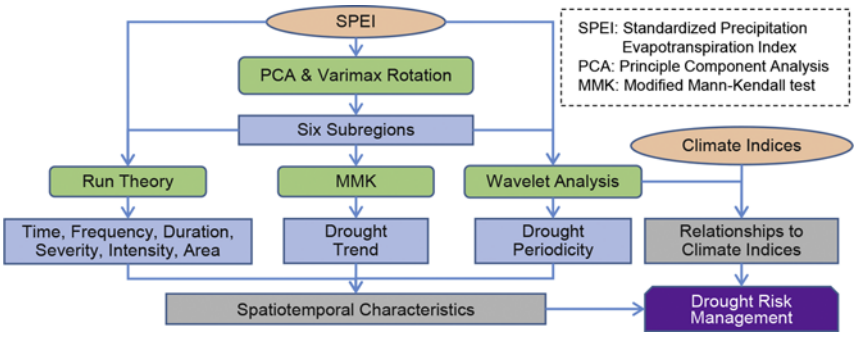

ARTICLE INFO

Article history:
Received 8 September 2017
Received in revised form 9 November 2017
Accepted 11 December 2017
Available online xxxx

Editor: G. Ashantha Goonetilleke

Keywords:
Drought characteristics
SPEI
Run theory
Drought trend
Drought periodicity
Teleconnection

ABSTRACT

In drought-prone regions like Central Asia, drought monitoring studies are paramount to provide valuable information for drought risk mitigation. In this paper, the spatiotemporal drought characteristics in Central Asia are analyzed from 1966 to 2015 using the Climatic Research Unit (CRU) dataset. Drought events, as well as their frequency, duration, severity, intensity and preferred season, are studied by using the Run theory and the Standardized Precipitation Evapotranspiration Index (*SPEI*) at 3-month, 6-month, and 12-month timescales. The Principle Components Analysis (PCA) and the Varimax rotation method, the Sen's slope and the Modified Mann-Kendall method (MMK), as well as the wavelet analysis are adopted to identify the sub-regional drought patterns and to study the drought trend, periodicity and the possible links between drought variation and large-scale climate patterns, respectively. Results show that the drought characteristics in Central Asia vary considerably. The Hexi Corridor region and the southeastern part suffered from more short-term drought occurrences which mostly occurred in summer while the northeastern part experienced fewer droughts with longer duration and higher severity. Central Asia showed an overall wetting trend with a switch to drying trend since 2003. Regionally, the continuous wetting trend is found in north Kazakhstan while a consistent drying in the Aral Sea and Hexi Corridor region is observed in the last half-century. For 2003–2015, a significant drying pattern is detected in most Central Asia, except the northern Kazakhstan. A common significant 16–64-month periodical oscillation can be detected

* Corresponding author at: State Key Laboratory of Desert and Oasis Ecology, Xinjiang Institute of Ecology and Geography, Chinese Academy of Sciences, Urumqi 830011, China.
E-mail addresses: guohao13@mails.ucas.ac.cn (H. Guo), baoam@ms.xjb.ac.cn (A. Bao), liutie@ms.xjb.ac.cn (T. Liu), glmr@ms.xjb.ac.cn (G.· Jiapaer), davfelix@radi.ac.cn (F. Ndayisaba), alishir@ms.xjb.ac.cn (A. Kurban), Philippe.DeMaeyer@UGent.be (P. De Maeyer).

https://doi.org/10.1016/j.scitotenv.2017.12.120
0048-9697/

over the six sub-regions. The drought changes in Central Asia are highly associated with ENSO but less related to the Tibetan Plateau pressure. The North Atlantic Oscillation has an influence on drought change in most Central Asia but less for the Hexi Corridor and the drought variation in eastern Central Asia is affected by the strength of the Siberian High.

1. Introduction

Drought is one of the most complicated but least understood natural hazards (Portela et al., 2015; Wilhite, 1996) with widespread impacts on water resources (Zhang et al., 2015), agricultural production (Al-Kaisi et al., 2013), ecosystem function (Bond et al., 2008), environment (Dijk et al., 2013), local and global economies (Ding et al., 2011). Generally, there are four types of drought: meteorological, agricultural, hydrological and socio-economic drought (Heim, 2002). Despite its widespread damages, drought identification and characterization are challenging due to its varying definition, great spatiotemporal variability, complicated physical process and non-structural impacts (Nam et al., 2012; Wu and Wilhite, 2004).

Over the past decades, lots of efforts have been devoted to drought monitoring and characterization and a series of drought indices has been developed, such as the Standard Precipitation Index (SPI) (McKee et al., 1993), Palmer drought severity index (PDSI) (Palmer, 1965), Rainfall Deciles (RD) (Gibbs, 1967), China-Z Index (CZI) (Wu et al., 2001) and Crop Moisture Index (CMI) (Palmer, 1968). Among them, SPI and PDSI are more popular and frequently used. As the first water-budget-based index, PDSI is considered as a landmark in the efforts dedicated to developing drought indices (Heim, 2002; Vicente-Serrano et al., 2010). It is calculated from precipitation, temperature and soil water content by considering both water supply and demand. However, it also faces many deficiencies like the fixed timescale, strong dependence on the data calibration, limitations in spatial comparability and the arbitrary interpretation of drought conditions to the index values (Andreadis et al., 2005; Sheffield et al., 2009; Wells et al., 2004). In order to overcome these shortcomings, the self-calibrating PDSI (scPDSI) was developed by Well et al. (Wells et al., 2004) and recently improved by Liu et al. (2017). However, the problem of fixed timescale has not been completely solved in scPDSI. Considering the important drought characteristics at multiple timescales, the SPI was developed with a lot of advantages, such as simple calculation, multiple timescales, good adaptability to different climates and an easy comparison between different regions. Owing to these advantages, the SPI has been widely applied to drought monitoring studies (Guo et al., 2016; Guo et al., 2017a; Vu et al., 2015; Zhu et al., 2016). However, SPI is only based on precipitation without considering temperature and evaporation which play an increasingly important role in drought occurrence as a result of global warming (Yoon et al., 2012).

The *SPE*I (Vicente-Serrano et al., 2010) was developed by not only considering the sensibility of droughts to temperature but also remaining the multiple timescales and allowing for flexible comparability. The calculation of *SPE*I is based on the water balance equation represented by the difference between precipitation (P) and potential evapotranspiration (PET). *SPE*I has been widely used in drought monitoring and characterization at the global and regional scales (Gao et al., 2017; Mallya et al., 2016; Paulo et al., 2012; Vicente-Serrano et al., 2010; Wang et al., 2014; Zhang et al., 2017). There are several methods for PET calculation and the Thornthwaite (1948) and Penman-Monteith (Allen et al., 1998) are currently the two most widely used equations. Since the Thornthwaite method is solely based on temperature, PET tends to be underestimated in the arid and semi-arid regions (Jensen et al., 1990). Due to the improved physical calculation process, the Penman-Monteith is widely accepted as the most accurate method to calculate PET (Gao et al., 2017). The superiority of Penman-Monteith over Thornthwaite in the calculation of *SPE*I has been confirmed by several studies (Chen and Sun, 2015; Gao et al., 2017). Therefore, considering the arid climate in Central Asia, the Penman-Monteith based *SPE*I is selected as the drought index in this study.

Central Asia (Kazakhstan, Kyrgyzstan, Tajikistan, Turkmenistan, Uzbekistan and the northwestern region of China) is characterized by the semi-arid and arid climate with scarce water resources (Qi and Kulmatov, 2008; Qi et al., 2012). Due to the rise in water demand as a consequence of the growing population and the larger variability in water resources resulting from both global warming and intense human activities, water resources in Central Asia are increasingly under pressure (Issanova and Abuduwaili, 2017a; Lubin, 2016; Qi et al., 2012). It has been proven that there is a significant increase in temperature and a small decrease in precipitation over Central Asia during the recent decades (Lioubimtseva and Cole, 2006; Lioubimtseva and Henebry, 2009; Xu et al., 2016; Yin et al., 2016). The effects of droughts will be aggregated due to the decreased precipitation and the increased evaporation (Sheffield and Wood, 2008). In addition, the uncontrolled human activity may also intensify the drought occurrences. For example, the desiccation of the Aral Sea has greatly impacted the local climate with more than three-time drought occurrences (Issanova and Abuduwaili, 2017b). Furthermore, most parts of Central Asia are vulnerable to droughts due to the extreme continental climate, a high dependence on irrigated agriculture and growing population (Bank, 2005). Despite the increasing drought risk, the study on droughts in Central Asia has received limited attention in recent years. For instance, Barlow et al. (2002) discussed the relationship between drought condition and large-scale climate patterns during 1998–2001; Xu et al. (2016) studied the response of vegetation to summer droughts by using the 3-month *SPE*I from 2000 to 2012; Z. Li et al. (2017) studied the drought variation based on PDSI from 1961 to 2014 and found a drying trend in Central Asia during the last decade. The sub-regional study of drought behaviors is important given the differences in trends, evolution and spatiotemporal drought characteristics. However, most of the previous works that focused on drought in Central Asia paid no attention to the drought characteristics at the sub-regional scale. Besides, understanding the drought structure and characteristics, like duration, severity and intensity, is crucial in the reduction of drought vulnerability and the establishment of drought adaptation strategies. But previous studies that studied drought trend or drought impacts were simply based on drought indices such as SPI, PDSI, or *SPE*I, and failed to extract drought events and to furtherly studied their structure and characteristics.

The general objective of this study is, therefore, to comprehensively analyze the spatiotemporal characteristics of drought events over Central Asia at the sub-regional scale based on CRU dataset and *SPE*I index during 1966–2015. Specifically, the objectives of this study are: (1) to identify the sub-regions with distinct drought characteristics by using PCA and the Varimax rotation method; (2) to find out drought events and characterize their properties (e.g. drought duration, severity, intensity and frequency) based on the Run theory; (3) to check the drought trend and periodicity based on the Sen's slope, the Modified Mann-Kendall and the Cross Wavelet Transform; (4) to delineate the possible relationship between drought variability and four related climatic indices using the Cross Wavelet Coherence analysis. The findings of this

study are promising to provide some valuable scientific reference for drought risk mitigation in Central Asia.

2. Materials and methods

2.1. Study area

The study area includes five countries (i.e. Kazakhstan, Kyrgyzstan, Tajikistan, Turkmenistan, and Uzbekistan) and the northwest China, which is referred to as Central Asia in this study (Fig. 1). The geography of Central Asia is complex and consists of high mountains (e.g. the Tianshan Mountain and the Karakoram mountain), low basins (e.g. the Tarim basin), vast deserts or Gobi (e.g. the Kara Kum, Kyzyl Kum and Taklimakan desert) and treeless grasslands (e.g. The north part of Kazakhstan) (Li et al., 2015; Mughal, 2013). The elevation ranges from less than −130 m in the Turpan Depression and the Karagiye Depression to >7500 m in the Pamir and the Karakoram mountains. Due to the inland position and remoteness from oceans, Central Asia is characterized by semi-arid and arid climate with low relative humidity and persistent soil moisture deficit (Qi and Kulmatov, 2008; Qi et al., 2012). Therefore, this region is one of the aridest regions in the world. As result of climate change and human activities, Central Asia is experiencing an increasingly severe deficit of water resources with increasing temperature and variable precipitation pattern (Guo et al., 2015; Guo et al., 2017b; Jiang et al., 2017). For example, the quick shrinking of the Aral Sea has attracted particular attention from the scientific community.

2.2. Datasets

2.2.1. CRU

Compared to the traditional gauge observations, the gridded dataset has a better spatial representativeness and continuous availability, which play an important role in characterizing droughts (Cheng et al., 2015; Thavorntam et al., 2015; Z. Wang et al., 2017). The monthly precipitation and potential evaporation data from the latest version of Climatic Research Unit Version 4.00 (CRU TS4.00) are used in this study for the period from 1966–2015. The CRU dataset is developed by the Climatic Research Unit (University of East Anglia) and is available online (http://www.cru.uea.ac.uk/data/). The CRU dataset is selected to calculate *SPEI* for several reasons: Firstly, the CRU dataset is based on a large number of stations with good quality control and homogeneity check (Mitchell and Jones, 2005). Secondly, the 0.5°-monthly spatial-temporal resolution and long-term (>100 years) availability satisfy the requirements for drought study and robust calculation of *SPEI* requiring at least 30 years of records (Burroughs, 2003). In addition, the PET data in CRU is calculated based on the Penman-Monteith equation which is the most accurate PET equation. Recent studies (Deng and Chen, 2017; Li et al., 2016; Z. Li et al., 2017) suggested that the CRU dataset is applicable and satisfactory for climatological studies in Central Asia. However, the CRU data before 1960 may not be suitable for different applications because a limited number of stations were included (Jones et al., 2016). Therefore, the data from 1966 to 2015 (50 years) is chosen for use in this study.

2.2.2. Climate indices

The climate of Central Asia is mainly affected by three factors: the Arctic and North Atlantic Oscillation (AO/NAO), the Siberian High (SH) and the Tibetan Plateau (TP) (Groll et al., 2013; Issanova and Abuduwaili, 2017a). It has been proven that the El Niño-Southern Oscillation (ENSO) phenomenon has a close relationship with drought occurrence in Central Asia (Barlow et al., 2002; Hoerling and Kumar, 2003). Therefore, the North Atlantic Oscillation (NAO), Siberian High Index (SHI) and Tibetan Plateau Index (TPI), as well as ENSO SST index (NINO34) are considered so as to investigate the relationship between drought variation and large-scale climate patterns. The summary of the four indices is demonstrated in Table S1.

The NAO plays an important role in the climate system of Central Asia. It has a close link with the Siberian High. When the NAO index is in a positive (negative) phase, the SH will be higher (lower) than the normal condition (Bingyi and Jia, 2002; Duan and Wu, 2005). The NAO index is defined as the difference of the sea level pressure (SLP) between the Subtropical (Azores) High and the Subpolar Low. It is provided by the NOAA Climate Prediction Center.

The SH is a strong anti-cyclone circulation system formed by the Mongolia-Siberian region (Panagiotopoulos et al., 2005). It can affect the climate of the northern and eastern part of Central Asia strongly by deflecting westerly cyclones and controlling the strength of the winter Asia monsoon (Cohen et al., 2001; Gong and Ho, 2002; Lioubimtseva et al., 2005). Therefore, the SHI is included based on the regional sea level pressure within 80–120°E, 40–60°N (Gong and Ho, 2002) according to the following equations.

$$\mathrm{SHI} = \frac{\sum_{i=1}^{n} P_i \lambda \cos\varphi_i}{\sum_{i=1}^{n} \lambda \cos\varphi_i} \tag{1}$$

$$\lambda = \begin{cases} 1 & \text{if } P_i \geq 1028 \text{ hPa} \\ 0 & \text{if } P_i \leq 1028 \text{ hPa} \end{cases} \tag{2}$$

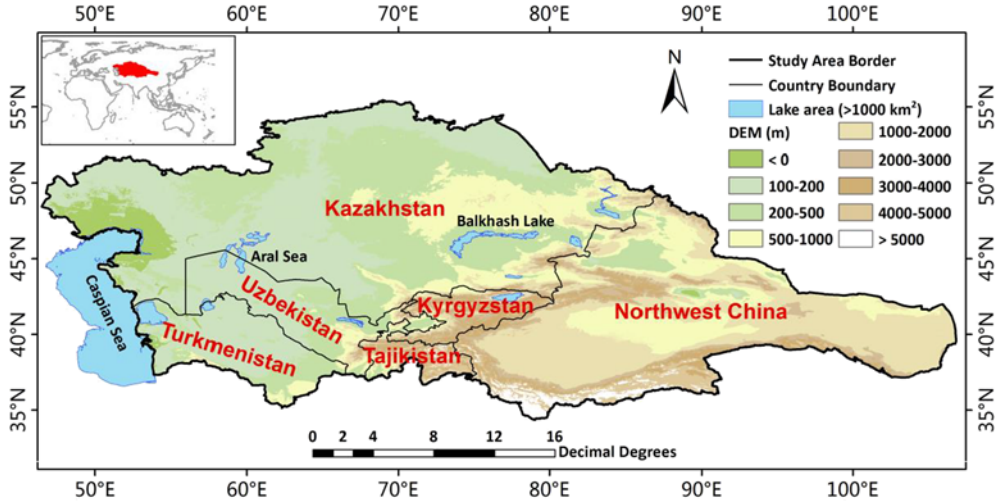

Fig. 1. Spatial distribution of elevation variation in Central Asia.

where *SHI* is the Siberian High Index; n is the number of grids located within the region; P_i is the sea level pressure in grid i; φ_i represents the latitude of grid i; λ is the flag defined in Eq. (2) according to Gong and Ho (2002).

The TP has a great influence on the atmospheric circulation in Central Asia by diverting the westerlies and affecting the Asian monsoon. It plays a role of towering heat source in the surrounding climate. The TPI is adopted in this study to describe the geopotential high strength of the Tibetan Plateau. The TPI is calculated from the accumulation of the product of the total grid area and the geopotential height difference between the value of grid and 5000 gpm in the region of 30°N–40°N, 75°E–105°E.

The NINO34 is one typical index considering the effect of ENSO on the climate. The NINO34 is defined as the average SST within the region bounded by 5°N–5°S and 170°W–120°W. The data is calculated based on the Met Office Hadley Centre's sea ice and sea surface temperature (SST) dataset (HadISST1) (Rayner et al., 2003), which is available in the National Oceanic and Atmospheric Administration (NOAA) Earth System Research Laboratory (ESRL).

2.3. Methods

2.3.1. SPEI

Due to its multiple advantages, *SPE*I is adopted in this study as the drought index. *SPE*I is based on the simple climatic water balance expressed by the difference between P and PET. The calculation procedure is described in the following steps. The first step is the calculation of the difference between P and PET in Eq. (3).

$$D_j = P_j - PET_j \tag{3}$$

where j is the month number, D_j means the difference between precipitation in month j (P_j) and *PET* in month j (PET_j). The second step is the aggregation and normalization of D_j at different timescales according to Eqs. (4) and (5). The normalization of $X^k_{i,j}$ is based on the log-logistic distribution function and the parameters for the log-logistic equation are calculated from the L-movement procedure as suggested by Vicente-Serrano et al. (2010).

$$\begin{cases} X^k_{i,j} = \sum_{l=13-k+j}^{12} D_{i-1,l} + \sum_{l=1}^{j} D_{i,l} & if \;\; j<k \\ X^k_{i,j} = \sum_{l=j-k+1}^{j} D_{i-1,l} & if \;\; j>k \end{cases} \tag{4}$$

where $X^k_{i,j}$ signifies the aggregated difference between P_j and PET_j at the k-month timescale in the jth month of the ith year.

$$F(X) = \left[1 + \left(\frac{\alpha}{X-\gamma}\right)^{\beta}\right]^{-1} \tag{5}$$

where α, β, and γ represent the scale, shape, and origin parameters, respectively. The α, β, and γ can be calculated by the L-moment procedure (Vicente-Serrano et al., 2010).

Then the probability of a definite $X^k_{i,j}$ and the final *SPE*I value is calculated as Eqs. (6)–(8) as follows.

$$p = 1 - F(x) \tag{6}$$

$$w = \begin{cases} \sqrt{-2\ \ln p} & \text{if} \;\; p \le 0.5 \\ \sqrt{-2\ \ln(1-p)} & \text{if} \;\; p > 0.5 \end{cases} \tag{7}$$

$$\text{SPEI} = \frac{C_0 + C_1 w + C_2 w^2}{1 + d_1 w + d_2 w^2 + d_3 w^3} - w \tag{8}$$

where $C_0 = 2.515517$, $C_1 = 0.802853$, $C_2 = 0.010328$, $d_1 = 1.432788$, $d_2 = 0.189269$, and $d_3 = 0.001308$. These parameters are defined in the study of Vicente-Serrano et al. (2010).

Positive *SPE*I indicates wet condition and negative *SPE*I signifies dry condition. Generally, the *SPE*I values at different timescales have a different sensibility to the dry/wet condition. As one attractive feature of *SPE*I, the flexibility in timescales enable *SPE*I to reflect different types of droughts like the short-term meteorological droughts and the long-term hydrological droughts (Ashraf and Routray, 2015; Mishra and Singh, 2010). In this study, *SPE*I at 3-month, 6-month and 12-month timescales (*SPE*I3, *SPE*I6, and *SPE*I12, respectively) are selected to depict the short-, intermediate- and long-term drought characteristics. Following Q. Wang et al. (2015), the dry/wet conditions based on *SPE*I are categorized in Table S2.

2.3.2. Drought identification and characteristics

Proposed by Yevjevich (1967), the Run theory is one of the most frequently used methods for drought event characterization (Liu et al., 2015). A run is defined as a portion of time series of the variable, in which all values are below one selected threshold (Lee et al., 2017; Montaseri and Amirataee, 2017). The runs can be both positive and negative. Following McKee et al. (1993), the drought event in this study is defined as continuous negative *SPE*I values for at least three consecutive months with the lowest *SPE*I less than −1. There are two reasons for this definition. Firstly, the consistent low-intensity drought also can have a great impact on agriculture, vegetation growth and the local environment (Gregor, 2012; Sheffield and Wood, 2007; Venturas et al., 2016). Secondly, starting from negative *SPE*I values to identify drought events can be helpful for the improvement of drought early-warning system. One drought event is a negative run. Once the drought event is defined, it can be characterized in terms of drought duration (DD), drought severity (DS), drought intensity (DI), and drought peak (DP) based on the Run theory (Fig. S1). DD is the month number between the drought initiation time (DIT) and the termination time (DTT). DS is the positive sum of *SPE*I values during a drought event. DI is the average of *SPE*I values within the drought duration which is measured as the drought severity divided by drought duration. DP refers to the absolute lowest SPEI value on a drought peak time (DPT) during the drought event.

In order to investigate the spatiotemporal drought characteristics, a series of drought event indices are calculated based on drought events identified by the Run theory in each grid. The annual drought frequency (ADF) is the annual mean number of drought occurrence; mean drought duration (MDD, Eq. (9)), mean drought severity (MDS, Eq. (10)), mean drought intensity (MDI, Eq. (11)) and mean peak value (MDP, Eq. (12)) in individual grids are calculated using the simple arithmetic mean of the corresponding characteristics of a single drought event (DD, DS, DI, and DP, respectively). The drought initiation season is useful for the regional drought mitigation. Therefore, the drought frequent season (DFS) is also retrieved based on the initiation time of drought events. The drought frequent season significance is determined by the ratio between the drought occurrence number in one specified season and the total number of drought occurrence (S.Z. Huang et al., 2015; Mo, 2011). If the drought initiation seasons are evenly distributed, then the ratio should be 25%. In this study, the drought season ratio is defined as a double normal percentage (50%). Finally, the drought area (DA), also known as areal extent or spatial extent, refers to the maximum number of grids under drought and is expressed as a percentage of the total number of grids in the study area or sub-regions.

$$MDD = \frac{\sum_{i=1}^{N} DD_i}{N} \tag{9}$$

$$MDS = \frac{\sum_{j=1}^{N} DS_j}{N}, DS = \sum_{i=1}^{DD} |SPEI_i| \tag{10}$$

$$MDI = \frac{\sum_{j=1}^{N} DI_j}{N}, DI = \frac{\sum_{i=1}^{DD} |SPEI_i|}{DD} \tag{11}$$

$$MDP = \frac{\sum_{j=1}^{N} DP_j}{N}, DP = \max_{1 \le i \le DD} |SPEI_i| \quad (12)$$

where *DD* is the drought duration for one drought event, *i* means one month during drought event, $SPEI_i$ is the SPEI value in month *i*; *DS*, *DI*, and *DP* are drought severity, drought intensity, and drought peak value for one drought event, respectively; *N* is the number of drought events observed during study period, *j* represents one drought event, *MDD*, *MDS*, *MDI*, and *MDP* depict the mean drought duration, mean drought severity, mean drought intensity and mean drought peak value during the specified period.

In order to quantify the change of drought characteristics, the definitions of relative differences of annual drought frequency (RADF), mean drought duration (RMDD), mean drought severity (RMDS), mean drought intensity (RMDI) and mean drought peak value (RMDP) are introduced here as the difference between the periods 1966–2002 and 2003–2015 (the mean value in 2003–2015 minus the mean value in 1966–2002). The period division is based on the common turning point in a 25-year span smooth line for different sub-regions.

2.3.3. PCA

In this study, PCA is used to identify the sub-regions with a similar drought co-variability based on SPEI. PCA is a dimensionality reduction method capable to distill structural information and extract patterns with similar variance characteristics. It can use a few linearly uncorrelated principle components (PCs) to explain most of the total variance in original data based on the computation of the covariance matrix with the corresponding eigenvalues and eigenvectors (Raziei et al., 2009). The normalized eigenvectors, which are also called "loadings", represent the correlation between the original data and the time series of component scores. The Bartlett's test of sphericity (Bartlett, 1954) and the Kaiser-Meyer-Olkin (KMO) test (Kaiser, 1970) are employed to check the sampling adequacy to ensure the robust PCA computation. The number of PCs is decided based on the rule of thumb (North et al., 1982) and the scree plot (Cattell, 1966), as well as the cumulative proportion of variance explained by PCs. The satisfactory cumulative variance percentage is set about 70% (Di Lena et al., 2013; Huang et al., 2014; J. Huang et al., 2015; Li et al., 2012; Telesca et al., 2013).

In order to find a more stable localized drought pattern, the Varimax rotation method (Richman, 1986; von Storch and Zwiers, 2002) is applied to the selected PCs. The Varimax rotation can further maximize the variance of squared correlations between the rotated principle components (RPCs) and the variables and simplify the spatial patterns with similar temporal variations (J. Huang et al., 2015; Zhao et al., 2012). The threshold of 0.6 is used as a criterion to separate the study area into sub-regions (Portela et al., 2017; Raziei et al., 2012; Z. Wang et al., 2017).

Due to the prior ample description and wide application of the PCA method and the Varimax rotation method, more detailed formula and properties will not be extensively introduced here. The identification of sub-regions based on the PCA analysis could provide a further regional view of drought characteristics. In this study, the 12-month SPEI is selected to identify sub-regions because the 12-month timescale could keep the interannual variation characteristics and avoid the seasonal cycle (Liu et al., 2016; Raziei et al., 2009), while the shorter timescales are too sensitive and the longer timescales may easily miss some relevant drought events (Spinoni et al., 2014; Vicente-Serrano and Lopez-Moreno, 2005). Some studies have found that the 12-month scale is more suitable for regionalization based on the PCA method (Liu et al., 2016; Spinoni et al., 2014; Y. Wang et al., 2017). In fact, the identification of sub-regions is not greatly affected as the other scales (i.e. *SPEI*3, *SPEI*6) also show comparable spatial patterns of RPCs.

2.3.4. Modified Mann-Kendall trend test and Sen's slope

In order to capture the monthly drought trends and the corresponding significance, the Sen's slope and MMK trend test are applied in this study. Developed by both Mann and Kendall (Kendall, 1990; Mann, 1945), the Mann-Kendall significance test (MK) is a kind of non-parametric method to measure the significance of trends in a time series of samples. The non-parametric MK method is recommended by World Meteorological Organization (WMO) for the trend significance test in climatology studies (Mitchell Jr et al., 1966) due to its low sensitivity to the outliers, no requirements for the sample to conform a certain distribution and its allowance for the existence of missing values. However, the MK method tends to underestimate the sample variance because it suffers from the serial correlation of time series as climatological and hydrological time series are serially independent (Suryavanshi et al., 2014; Yang et al., 2014). Therefore, Hamed and Rao (1998) proposed the MMK by adding a correction factor to the original variance computation based on the effective or Equivalent Sample Size (ESS) to avoid the effect of the temporal data auto-correlation. It has been proven that the MMK is more reliable and robust than the original MK method for capturing the trend in hydrometeorological studies (Daufresne et al., 2009). The detailed computation procedure may refer to the studies of Daufresne et al. (2009) and Tabari et al. (2014).

The Sen's slope is another non-parametric method which allows missing values and has no requirements for data to conform to a particular distribution. The trend steepness is measured by the median of slope (Q_{med}). The detailed calculation has been given in Sen's study (Sen, 1968). The Sen's slope is usually applied to quantify the true slope of MK trend analysis (Da Silva et al., 2015; Joshi et al., 2016). In this paper, the Sen's slope method is used to measure the slope magnitude and the MMK method is applied to determine the significance at a 0.05 level.

2.3.5. Continuous wavelet analysis

Wavelet analysis is used to identify and describe the dominant localized variations in time series by decomposing data into time and frequency space (Grinsted et al., 2004). Compared to the Fourier analysis, the continuous wavelet analysis is superior for its self-adjusted time resolution, flexible mother wavelet, and suitability for non-stationary time series (Maraun and Kurths, 2004; Torrence and Compo, 1998). Due to the above mentioned advantages, wavelet analysis has been widely applied to study the drought periodicity and relationships between drought condition and teleconnections (Huang et al., 2016; Huang et al., 2017; Joshi et al., 2016; Liu et al., 2013; Merino et al., 2015; Mishra et al., 2015; Wang et al., 2015b; Zhao et al., 2017).

In this study, the continuous wavelet transform (CWT) is used to identify the periodicity of droughts and the wavelet coherence (WCO) is adopted to analyze the teleconnection between drought variation and large-scale climate patterns. The CWT is used to find the high common power and the phase relationship between drought variation and climate indices, while the WCO is applied to identify the local high correlation between the drought variation and the climate indices. The Morlet mother wave is adopted in the wavelet analysis due to its reasonable localization for both time and frequency (Grinsted et al., 2004). The CWT and WCO analysis are tested by the Monte Carlo method at a 0.05 statistical significance level (Grinsted et al., 2004; Maraun and Kurths, 2004). In order to eliminate the influence cone effect (edge effect), the significant coherence is identified by the threshold of $T/2\sqrt{2}$, where T represents the length of time series (Maraun and Kurths, 2004). For WCO, the phase relationship between two time series is indicated by directional arrows: the right arrow means in phase and the left arrow indicates anti-phase; the up arrow implies climate indices leading *SPEI* by 90°; the down arrow suggests *SPEI* leading climate indices by 90°. For a more detailed explanation of the theory of continuous wavelet analysis, one may refer to Maraun and Kurths (2004). The MATLAB package of wavelet analysis is provided by Grinsted et al. (2004).

3. Results and discussion

3.1. PCA regionalization

Based on the PCA and the Varimax rotation method, *SPEI*12 is used to identify the sub-regional drought patterns. In order to assess the sampling adequacy, both Bartlett's test of sphericity and the KMO test are applied to the *SPEI*12 time series. The low Bartlett's test *p*-value (<0.001) and high value of the KMO test (0.86) indicate that the *SPEI* time series is well qualified for the PCA analysis. Based on the rule of thumb and the scree plot of eigenvalues, the first six PCs with a cumulative percentage of 67.2% are selected for the maximum Varimax rotation (Table S3) to obtain more stable regionalized patterns. Because the seventh PC is found not robust enough for regionalization with eigenvector values ranging from −0.35 to 0.59 (<0.6). It is shown that the cumulative variance percentage of the RPCs is unchanged with the PCs, which indicates that the total variance of PCs is evenly explained by the six RPCs.

In order to study the drought characteristics at a sub-regional scale, Central Asia is separated into six sub-regions with different drought variation based on the border of RPCs with a threshold of 0.6 (Fig. 2). To validate the regionalization, the Spearman Correlation Coefficients (CCs) between the scores for six RPCs and the *SPEI* mean values in the corresponding sub-regions are given in Fig. 2. Here the Spearman method is selected as it is a non-parametric test. The high CCs (>0.81) suggest that the separation of sub-regions is adequate for studying the local drought characteristics. For brevity, the six sub-regions from RPC1 to PRC6 are named according to their positions in Central Asia: the southwest (SW), the north Kazakhstan (NK), the northeast (NE), the southeast (SE), the Hexi Corridor (HX) and the northwest (NW).

3.2. Drought characteristics

3.2.1. Temporal characteristics

The temporal evolution of *SPEI* in different sub-regions at various timescales may help us to understand the temporal variation of droughts at a sub-regional scale. Fig. 3 shows the temporal evolution of *SPEI* based on grids over six sub-regions at different timescales (i.e. SPEI3, SPEI6, and SPEI12). In order to capture the linear and nonlinear patterns of SPEI, the linear trend line and the local regression (LOESS) curves with a 5-year and 25-year time span are fitted to SPEI time series at different timescales. The linear line, 5-year and 25-year LOESS curves are marked by the solid blue line, the solid green and red line, respectively. In addition, the local turning points are detected based on the 5-year and 25-year LOESS curves by using the findpeaks MATLAB function.

As the timescale increases, the amplitude and the frequency of fluctuation decrease while the separations between dryness and wetness become clearer (Fig. 3). Despite the great detected difference in fluctuation frequency, the 5-year and 25-year smoothed lines as well as the linear trend line, show similar patterns between different timescales.

According to the pattern of 25-year LOESS curves, NW, NK, SW, and NE experienced dryness with relatively lower SPEI values in the 1970s and 1990s while SE and HX suffered from dryness in the 1980s as shown in Fig. 3. The dry periods detected in NW, NK, SW, and NE are consistent with the study of Xu et al. (2017). Based on linear trend lines, SW and HX remain stable or slightly dry whereas the other regions (NW, NK, NE, and SE) become wet in the global period (1966–2015).

It is obvious that there is a common turning point around 2003 in Central Asia at different timescales (SPEI3, SPEI6, and SPEI12) in Fig. 4a–c. The 2003 turning point is also detected in five sub-regions based on 5-year and 25-year LOESS curves at various timescales. However, in SE, only the 2003 turning point based on 5-year LOESS curves is found (Fig. 4p–r). An obvious wetting trend with a larger magnitude is found in NK after 2003 (Fig. 3d–f). In contrary, a drying tendency is detected in other sub-regions (i.e. NW, SW, NE, SE, and HX) after 2003. The local turning point in 2003 is also found by Xu et al. (2017) based on the Global Precipitation Climatology Center dataset (GPCC). The drying trend in the recent decade was also found by Z. Li et al. (2017b). Based on the common turning point of 2003, the period from 2003 to 2015 (13 years) is isolated to pay more attention to the recent drying trend over Central Asia and its sub-regions.

To quantify the drought trend during 1966–2015 and 2003–2015, the Sen's slope and MMK significance test results based on the mean SPEI are listed in Table S4. The results are consistent with the global linear line and the patterns of the LOESS curves shown in Fig. 3. *SPEI*s in NK show significantly negative slopes (-0.56×10^{-3} for SPEI3, -0.75×10^{-3} for SPEI6 and -0.67×10^{-3} for SPEI12 during 1966–2015; -4.44×10^{-3}, -5.42×10^{-3} and -5.48×10^{-3} during 2003–2015) at a 0.01 significance level for all three timescales and the

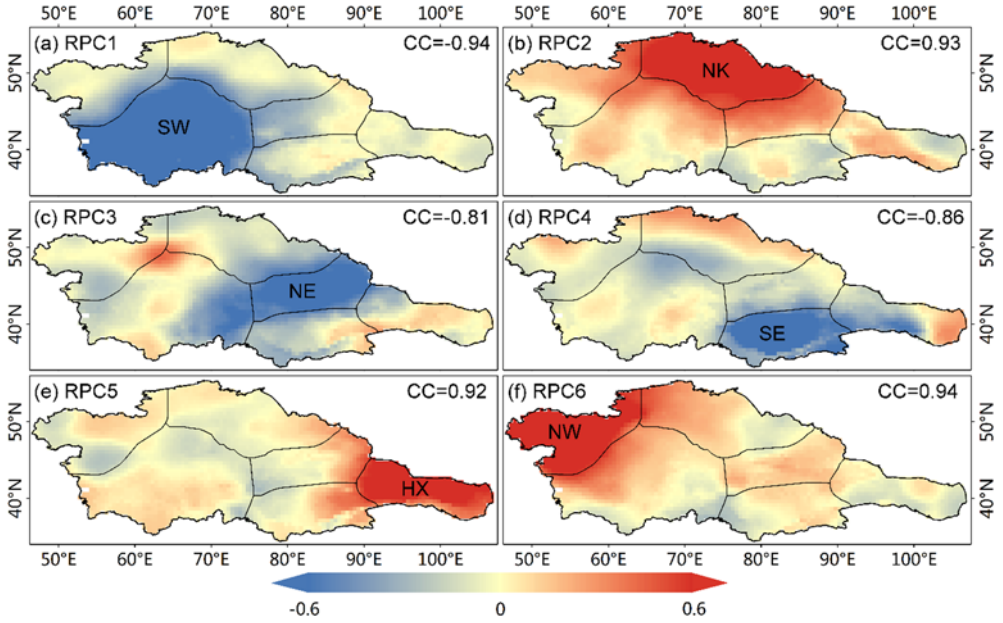

Fig. 2. The first six Varimax rotated components (RPC) of *SPEI*12. The black solid lines indicate the sub-regions based on the spatial pattern of the first six RPCs. CCs are the Spearman Correlation Coefficient values between PC scores and the spatial averaged *SPEI* over six sub-regions.

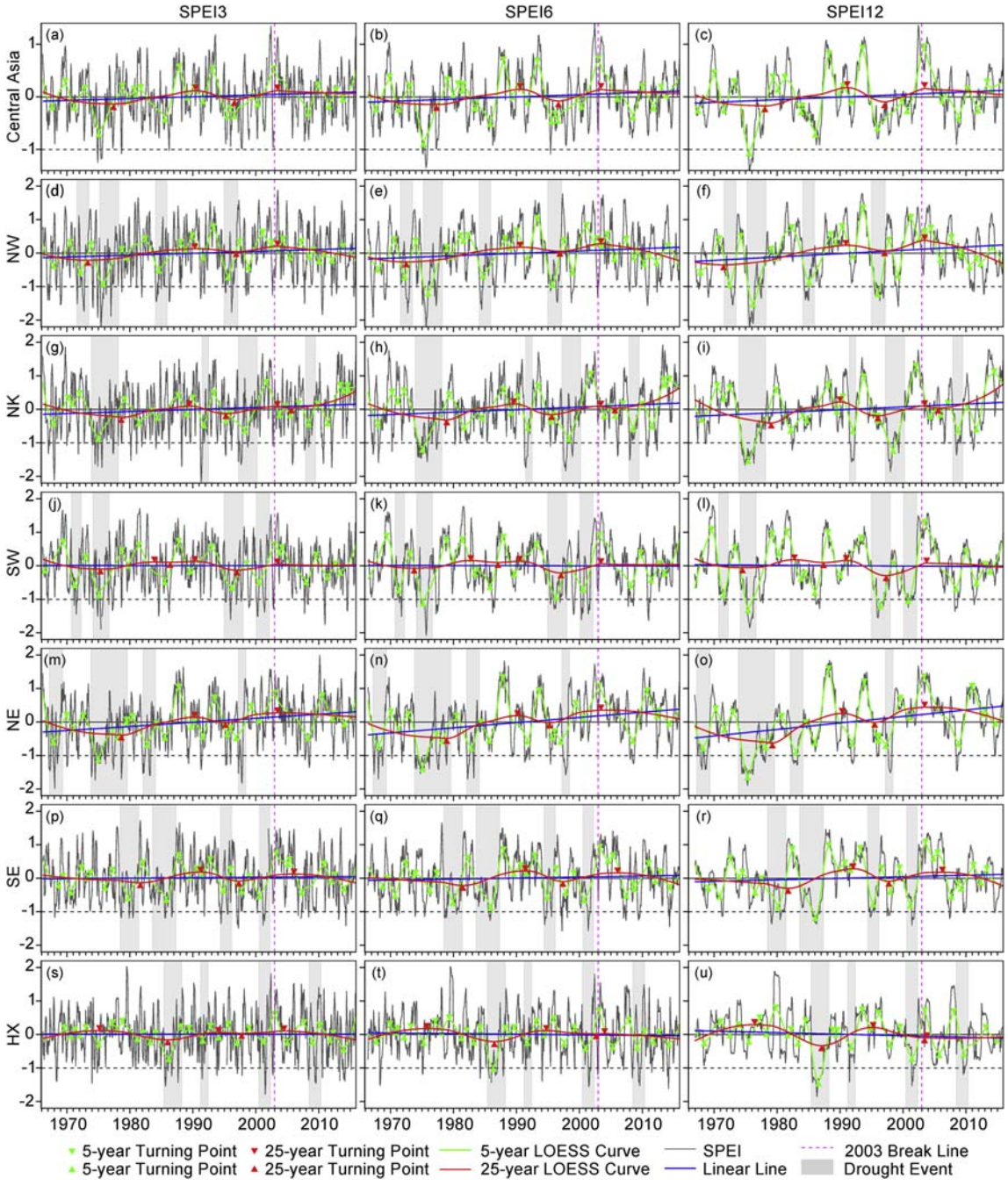

Fig. 3. Temporal evolution of SPEI at different timescales (SPEI3, SPEI6, and SPEI12) over Central Asia and six sub-regions. The linear trend line and smoothed lines based on locally regression (LOESS) with a time span of 5-year and 25-year are fitted and marked by the blue, green and red solid lines, respectively. The corresponding red and green triangles are the turning points based on the LOESS curves with a 5-year and 25-year time span, respectively. The dashed magenta line represents the year of 2003 for better comparison before and after. The gray rectangles highlighted in different plots indicate the periods when the four most severe drought events occurred. (For interpretation of the references to color in this figure legend, the reader is referred to the web version of this article.)

slope magnitudes during 2003–2015 are much higher than in the global period of 1966–2013. This indicates that NK has experienced a continuous wet period during the last half-century, and the wetting trend has become more intense during the latest 13 years. Contrary to NK, the continuously negative slopes are detected over HX sub-region, but only the period of 2003–2015 for SPEI3 and the period of 1966–2015 for SPEI12 have passed the significance test at a level of 0.1. All the other regions (NW, NE, and SE) show negative slopes throughout the period of 1966–2015 and positive slopes with a larger magnitude during 2003–2015. Especially, the slope of SPEI12 over NW, SW, NE, and SE has passed the significance level of 0.1, which indicates that these regions show a significant drying trend during 2003–2015.

Generally, during the period of 1966–2015, NK is dominated by a continuously significant wetting trend while HX displays a slightly drying trend. In contrary to the wetting trend during 1966–2015, the significant positive trend is found for the regions of NW, NE, and SE in the period of 2003–2015.

Drought area is one important characteristic of drought events; it can be used to measure the drought severity. To further investigate the temporal characteristics of droughts over different sub-regions,

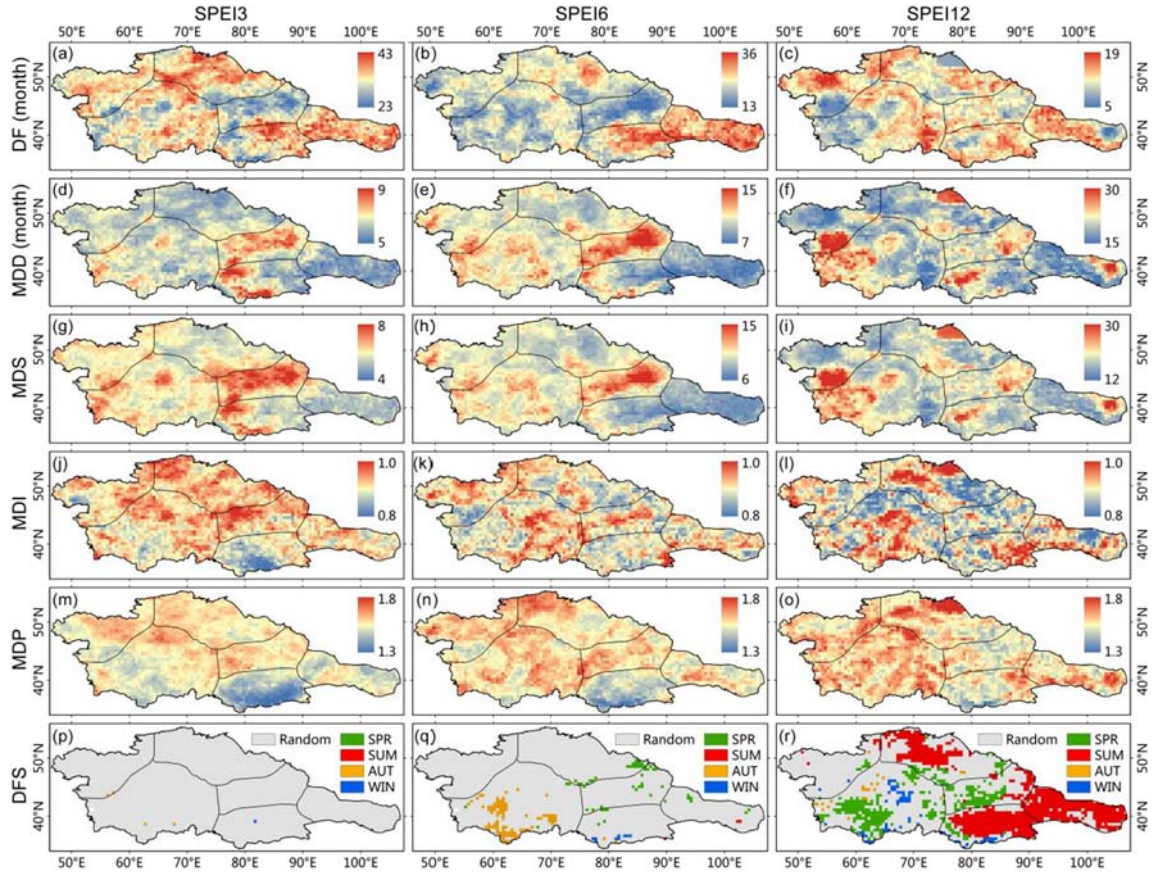

Fig. 4. Spatial patterns of drought characteristics for different timescales during 1966–2015: (a–c) Drought Frequency (DF), (d–f) Mean Drought Duration (MDD), (g–i) Mean Drought Severity (MDS), (j–l) Mean Drought Intensity (MDI), (m–o) Mean Drought Peak (MDP) and (p–r) Drought Frequent Season (DFS).

the temporal variations of area percentage affected by moderate, severe and extreme droughts are shown in Fig. S2. The drought area is relatively high in the 1970s and 1990s in regions of NW, NK, SW, and NE while a high area percentage ratio is found in the 1980s for SE and HX regions. It is noted that the drought areas in NE, SE, and HX have had smaller fluctuations since the middle 1980s. This is consistent with the fact that the northwest of China has been getting wetter since 1986 (Wang et al., 2015b; Zhang et al., 2012). Despite a relatively lower drought area percentage for the period after 2003, a slow increase in the drought area has also been detected in NW, NE, and SE (Fig. S2a–c and j–o); exhibiting a close agreement with the results of Fig. 3 and Table S4.

3.2.2. The most severe drought events

Based on the region-averaged SPEI12, the four most severe drought events (D1-D4) are identified and the corresponding drought characteristics are calculated in six sub-regions (Table 1). The drought events are marked by the gray rectangles in each plot of Fig. 3 and Fig. S2. It is noted that the drought events listed in Table 1 for each sub-region are sorted from high to low according to the drought severity.

Most severe drought events are detected within the dry periods for each sub-region, such as the period before 1980 and the period from 1993 to 2003 for NW, NK and SW and the 1980s for SE and HX. Among these drought events, some occurred across several sub-regions. The most severe drought events in NW, NK, SW, and NE are identified from 1973 to 1979 with a drought duration of >31 months and a drought peak in 1975, having a drought-affected area amounting to >93% (100% for NW, 98.82% for NK, 95.14% for SW and 93.64% for NE). The 1975 drought event is reported as one of the most severe droughts of the 20th Century (Y. Li et al., 2017; Sheffield and Wood, 2012). The duration of this drought event could last longer than 5 years (70 months) over SW, while the highest DI is detected over NW with a value of 1.07. The results indicate that most parts of Central Asia were affected by the most severe dryness in the last half century during the period of 1973–1979. Similarly, the most severe drought event in SE and HX is detected between 1983 and 1988 which is consistent with the previous report by Yu et al. (2017). Of special note is that a severe drought event is detected between 1997 and 2003 from the north (NK during April 1997–April 2000, NE during April 1997–January 1998) to the south (SW, SE, and HX for the period of 2000–2002) with a drought intensity of >0.72. The long-term severe drought event had caused great damage to the agriculture and economy in Central Asia as reported by previous studies (Bank, 2005; Hoerling and Kumar, 2003; Mariotti, 2007). These events can also be clearly observed in Fig. 3.

3.2.3. Spatial characteristics

Assessing the spatial drought characteristics is crucial for understanding droughts (Andreadis et al., 2005). In this paper, the spatial distributions of drought characteristics (i.e. DF, MDD, MDS, MDI, MDP, and MFS) are shown in Fig. 4. As the timescale increases, DF decreases from 23–43 times for *SPEI*3 to 5–19 times for SPEI12, whereas the MDD and MDS increase from 5–9 months to 15–30 months and from 4–8 to 12–30, respectively.

Except for differences between timescales, there are also some common features. Obviously, the regions of HX and the eastern part of SE are characterized by relatively higher DF and relatively lower MDD and MDS, which indicates that the region experienced more drought events but of relatively short duration and lower severity. This result agrees well with the frequent fluctuations of SPEI in SE (Fig. 3m–p) and HX (Fig. 3q–r) and the relatively dense drought area pillars as shown in Fig. S2m–p for SE and Fig. S2q–r for HX. In contrast, the NE sub-region suffered from lower DF but relatively longer DD and larger DS. At the 12-month scale, the west part of SW and the south part of NW (region

Table 1
The drought characteristics of the four most severe drought events that occurred in the six sub-regions based on SPEI12 during the period from 1966 to 2015. Drought events in each sub-region are sorted out based on the drought severity from high to low. The same color indicates drought events that occurred within the similar time period in different sub-regions.

Region	Event	Initiation time	Peak time	Termination time	DD (months)	DP	DS	DI	DA (%)
NW	D1	Apr-1975	Sep-1975	Apr-1978	37	−2.23	39.67	1.07	100
	D2	Jan-1995	May-1996	Mar-1997	27	−1.42	24.83	0.92	89.15
	D3	Aug-1971	Jan-1973	Jul-1973	24	−1.54	19.54	0.81	83.98
	D4	Feb-1984	Jan-1985	Dec-1985	23	−1.42	17.22	0.75	86.05
NK	D1	Dec-1973	Dec-1974	Mar-1978	52	−1.67	49.22	0.95	98.82
	D2	Apr-1997	Jan-1998	Apr-2000	37	−1.85	30.65	0.83	93.5
	D3	Jul-1991	Nov-1991	Jul-1992	13	−1.57	14.88	1.14	90.75
	D4	Dec-2007	Jul-2008	Jul-2009	20	−1.36	13.50	0.67	72.24
SW	D1	Mar-1974	Sep-1975	Sep-1976	31	−1.85	30.03	0.97	95.14
	D2	Jan-1995	Feb-1996	Jan-1998	37	−1.55	29.18	0.79	79.86
	D3	Feb-2000	Nov-2000	Mar-2002	26	−1.24	20.96	0.81	63.98
	D4	Oct-1970	Sep-1971	Apr-1972	19	−1.19	15.49	0.82	63.86
NE	D1	Nov-1973	May-1975	Aug-1979	70	−1.89	61.24	0.87	93.64
	D2	Apr-1967	Aug-1968	May-1969	26	−1.42	23.37	0.90	91.52
	D3	Feb-1982	Mar-1983	Feb-1984	25	−1.28	18.69	0.75	76.97
	D4	Apr-1997	Jan-1998	Jun-1998	15	−1.51	13.04	0.87	88.79
SE	D1	Aug-1983	Apr-1986	May-1987	46	−1.36	34.05	0.74	76.55
	D2	Jul-1978	Mar-1979	Jun-1981	36	−1.36	23.62	0.66	87.11
	D3	Jun-1994	Nov-1994	Mar-1996	22	−1.16	15.93	0.72	76.03
	D4	Aug-2000	Jun-2001	Apr-2002	21	−1.40	15.11	0.72	81.19
HX	D1	Jun-1985	May-1986	Apr-1988	35	−1.85	15.11	0.72	85.93
	D2	Jul-2000	Jun-2001	May-2002	23	−1.85	34.79	0.99	81.44
	D3	Jul-2008	Aug-2009	May-2010	23	−1.53	15.07	0.66	64.97
	D4	Apr-1991	Jul-1991	Jun-1992	15	−1.19	11.18	0.49	82.34

near the Caspian Sea) show relatively higher DS and DD but lower DF. However, this regional pattern is not obvious at 3-month and 6-month timescales. The patterns of MDI seem to be random and complex at different timescales (Fig. 4j–l). The drought peak values at different timescales in SE are found to be lower than in the other regions which may be related to the relatively more arid climate in the Taklamakan Desert (Fig. 4m–o).

As shown in Fig. 4p–r, the drought events seem to occur randomly at 3-month and 6-month timescales. However, in most parts of HX and SE, as well as some parts of NK, they tend to occur in summer at 12-month timescale as evidenced by the significantly high ratio (>50%) of summer-starting droughts (Fig. 4r). In addition, sparse green patches indicating a significantly high proportion of spring-starting droughts are also found in both NE and SW which suggest that the drought events in these areas tend to occur in spring.

Fig. 5 highlights the relative differences in terms of drought characteristics (RADF, RMDD, RMDS, and RMDI) between the two distinct time periods (1966–2002 and 2003–2015). The differences of RMDD and RMDS between two periods become larger as the timescale increases from 3-month to 12-month.

Generally, comparing to the period of 1966–2002, most of Central Asia experienced a relatively wet period during 2003–2015 with a lower magnitude of DF, DS, DD, and DI. However, some regional patterns with higher drought characteristics (i.e. DF, DS, DD, and DI) were also identified. The NW, HX and eastern part of SE experienced more drought events (about 0.03 time/year) with longer drought duration, higher drought severity and drought intensity in the latest 13 years at 3-month timescale, though the patterns of RMDD, RMDS, and RMDI are not obvious at 6-month and 12-month timescale. Of special concern are the common positive patterns in RMDD and RMDS (Fig. 5d–i) over the central part of SW (the Aral Sea region) without evident patterns of RADF and RMDI. The positive patterns of RMDD and RMDS are more obvious at 12-month timescales because the 12-month scale is more closely related to hydrological drought (Svoboda et al., 2012). The results indicate that the Aral Sea region suffered from droughts with long duration and large severity which is consistent with the severe desiccation of the Aral Sea in the last decade (Gaybullaev et al., 2012; Micklin, 2016).

3.3. Spatial drought trends

Fig. 6 shows the drought trend based on the Sen's slope and the Modified Mann-Kendall method at a 0.05 significance threshold. The color bar with gradient color from red to blue represents the magnitude of slope at a 10^{-3} scale. The red (blue) color indicates drying (wetting) trend. And the significance of dryness (wetness) is marked by red (blue) dots at a 0.05 significance level. In order to keep the clarity of the spatial patterns, different slope magnitudes are used for the two periods (1966–2015 and 2003–2015).

The spatial trend patterns at different timescales are similar. Central Asia shows an overall wetting trend resulting from the local drying trend (29%, 30%, and 34% of Central Asia for *SPE*I3, *SPE*I6, and SPEI12,

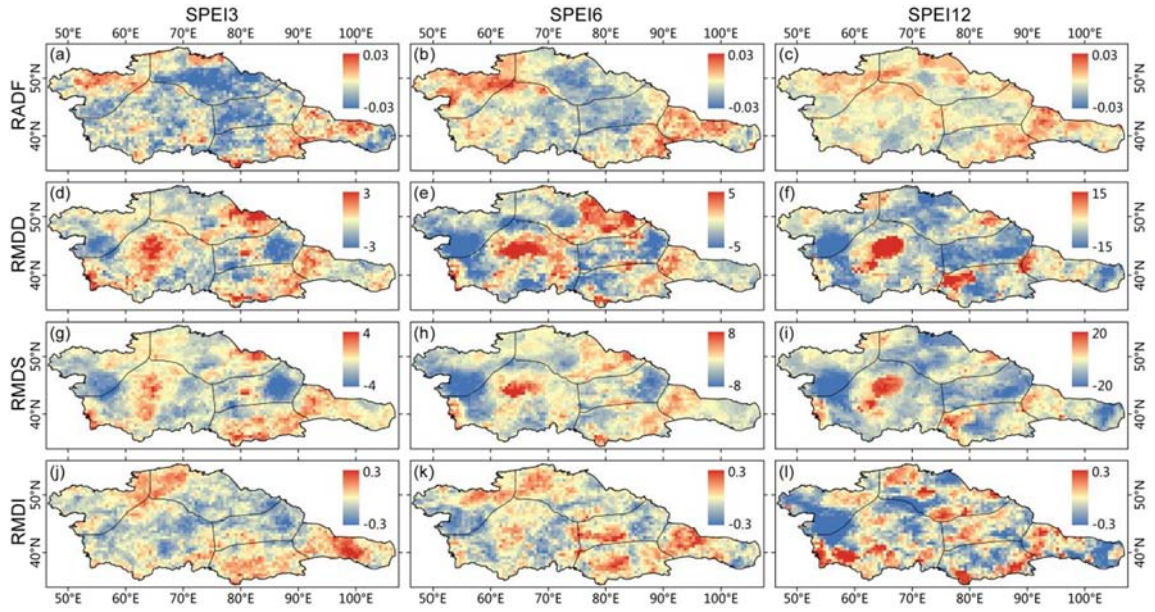

Fig. 5. Spatial distribution of relative difference of drought characteristics between the periods 2003–2015 and 1966–2002 at different timescales for (a–c) Relative Difference of Annual Drought Frequency (RADF), (d–f) Relative Difference of Mean Drought Duration (RMDD), (g–i) Relative Difference of Mean Drought Severity (RMDS) and (i–l) Relative Difference of Mean Drought Intensity (RMDI).

respectively) and the wetting trend (71%, 70%, and 66% of Central Asia for SPEI3, SPEI6, and SPEI12, respectively) during the period of 1966–2015. Specifically, a considerable wetting trend is found over NW, NK and NE sub-regions with wet area proportions of about 87%, 87%, and 100%, respectively. It is also noted that the whole NE (100% wet area) has a significant wetting change trend with a relatively large slope value (an obviously deeper blue color at SPEI12 timescale in Fig. 6e). The patterns over SW, SE, and HX are relatively complex with mixed wetting and drying trends. The central part of SW, the southern part of SE and the western part of HX tend to be dry with a drying area ratio of 46%–54%, 35%–41%, and 43%–66%. In addition, the substantial drying area over HX seems to become larger as the timescale increases from 43% to 66%. The mixed patterns can also be used to explain the relatively stable change detected in Fig. 3 based on the mean *SPEI*.

Within the period of 2003–2015, the patterns at different timescales are similar and can be clearly divided into two parts. One is the wetting change mainly covering NK with a wetting area ratio from 30% for SPEI12 to 34% for SPEI6, while the other part includes almost all the remaining regions (i.e. NW, SW, NE, SE, and HX) with drying area percentages from 66% for SPEI3 to 70% for *SPEI*12. The mixed patterns yield the overall drying trend over Central Asia during the period 2003–2015. The results are consistent with those shown in Fig. 3 as well as in Table 1. It should be noted that the drying trend in some parts of SW, NE, SE, and HX is not significant at a 0.05 significance level.

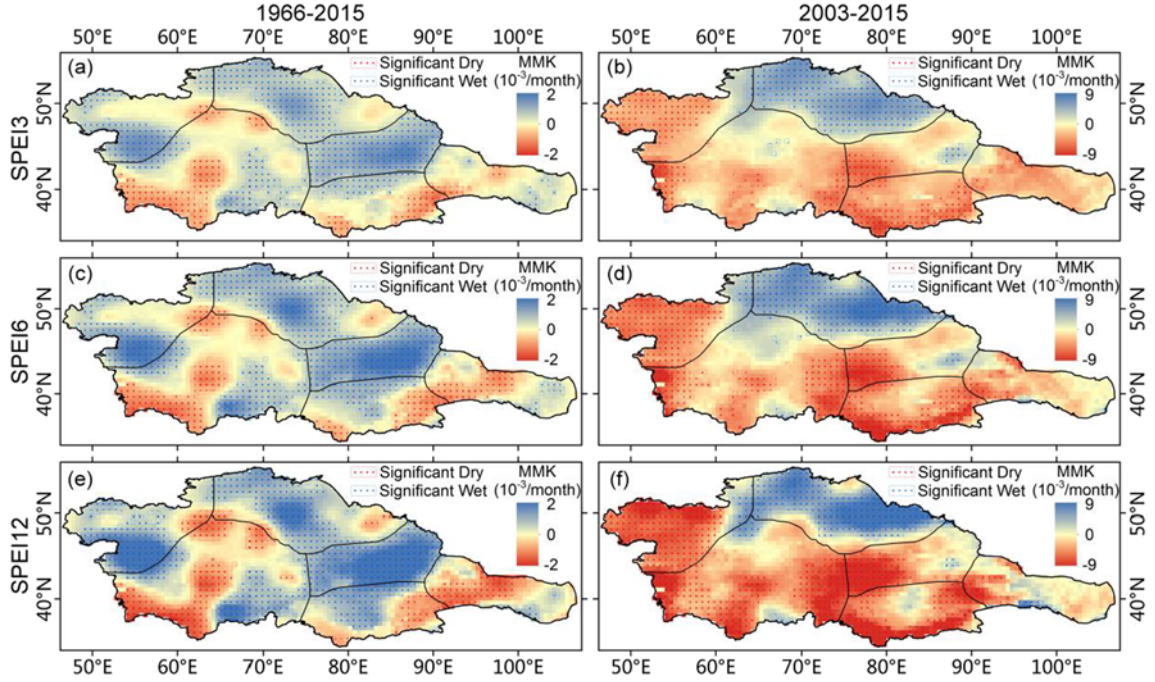

Fig. 6. Modified Mann-Kendall drought trend for *SPEI*3, SPEI6, and SPEI12 within the period of 1966–2015 and 2003–2015. (For interpretation of the references to color in this figure, the reader is referred to the web version of this article.)

Generally, Central Asia experienced a general wetting change during 1966–2015 with a recent drying trend in the latest 13 years (from 2003 to 2015). Specifically, the NK sub-region experienced a continuously wetting trend while the central part of SW and the western part of HX suffered from the persistently drying trend during the whole study period.

3.4. Drought periodicity

In order to identify the periodicity of drought variations, the wavelet power spectrums based on *SPEI*12 for six sub-regions are given in Fig. 7. The results of this section may be useful to explain the physical and dynamical mechanisms associated with the variability of drought events (Zeleke et al., 2017). In general, the periodicities of drought variation in the six sub-regions are mainly within the band of 15–64 months. Considerable differences between different regions are detected in the power patterns of the six sub-regions. Very few high-power variation periodicities <16 months are distributed in all regions.

For NW (Fig. 7a), a 16–55 months periodicity with decreasing amplitude is identified in the 1970s. It is interesting that the significant power regions are consistently distributed in 16–32 months period within the 1980s and 2000s, and 32–64 months period within the 1990s. The increasing frequency or decreasing periodicity after 2000 may at least partially explain the increasing drying trend discussed before (Fig. 6f). Different from other regions, the significant power patterns in NK are discrete. The drought variability band between 16–40 years occurred during both 1987–1993 and 2004–2013. The periodicities with 85–-110 months band are distributed in 1972–1982 and 1992–1999, the wavelet power between them is also high but does not reach the significance level (0.05). It is noteworthy that the recurring periodicities in SE are relatively stable with a wavelength of 15–45 months during the whole study period which indicates relatively smaller drought variation in this region. The significant wavelet power of around 64-month band is detected during 1988–2005 for SW, between 1987 and 1997 for NE, 1979–1990 for SE and 1998–2007 for HX. The 12-month *SPE*I in both NW and SW show a considerable amount of power with decadal variability (around 128-month) from 1880 to 2000 but they are not significant at a level of 0.05.

3.5. Links between drought variation and climate indices

Studying the links between the large-scale climate patterns and drought variation is helpful to understand the drought formation mechanism and evaluate the roles played by the atmospheric circulation variability on the characteristics of regional droughts (Wang et al., 2015a). Fig. 8 shows the wavelet coherence between different climate indices (including NAO, TPI, SHI, and NINO34) and spatially averaged SPEI12 over six sub-regions.

There is a discernible significant negative coherence between NAO and SPEI12 for a period of 6–10 months during 1973–1976 and 2010–2013, while an NAO leading coherence with a 110–128 months cycle band is also found from 1979 to 2000. These results indicate that the drought variation over NW is obviously influenced by NAO. Different from the NAO, the SHI has an in-phase relationship with drought variation in NW for 24–32 months during 1998–2015 and 32–64-month band in the period 1970–1975. These results are consistent with the fact that the SH is greatly affected by NAO with a negative correlation (Bingyi and Jia, 2002; Duan and Wu, 2005). TPI also exhibits significant correlations with drought variation in NW concentrated in 80–140 months band between 1978 and 1997.

Frequent short-period (5–12 months) coherences with a strong significance are detected in NK between NAO and SPEI for 1974, 1983, 1992, 1996, 2005 and 2011. Interestingly, the in-phase significant coherence is identified at both the interannual and decadal scale (i.e. 32–60 months band and 128–256 months band) for the period 1973–1984 and 1989–2000, respectively. Significant in-phase coherence can be observed within the band of 64–128 months during the period of 1970–1984, which indicates the co-variance between the drought variation and TPI in NK (Fig. 8g). It is noteworthy that there is an increasing coherence between SPEI and NINO34 for the band of 6–48 months since 2000 (Fig. 8h). This may suggest the increasing influence of NINO34 on the drought condition of NK after 2000.

As for SW, NINO34 shows a strong influence on drought variation as evidenced by a remarkable coherence pattern with an in-phase or NINO34 leading relationship in 28–64 months band during 1972–1976, 50–90 months band during 1989–2004 and 28–90 months

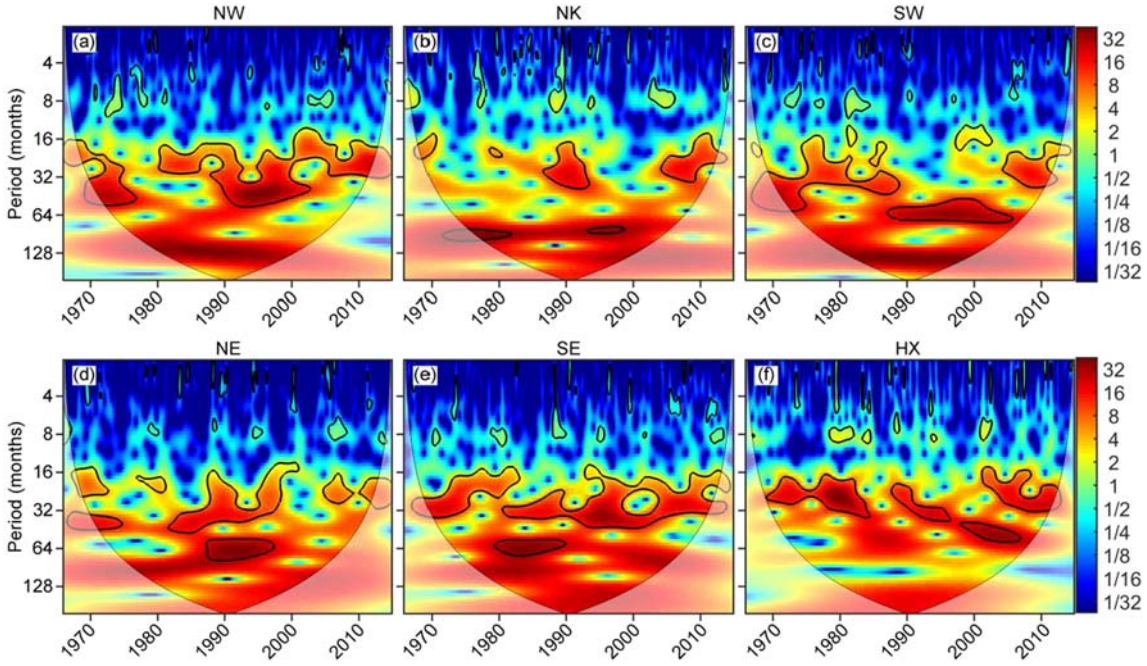

Fig. 7. The power spectrum of continuous wavelet transform (CWT) based on spatially averaged *SPEI*12 over six sub-regions from 1966 to 2015. The color from blue to red indicates the increasing wavelet power. The solid black contour represents the 0.05 significance level of local power relative to red noise and the light shade area means the cone of influence (COI) where the edge effects are not negligible. (For interpretation of the references to color in this figure legend, the reader is referred to the web version of this article.)

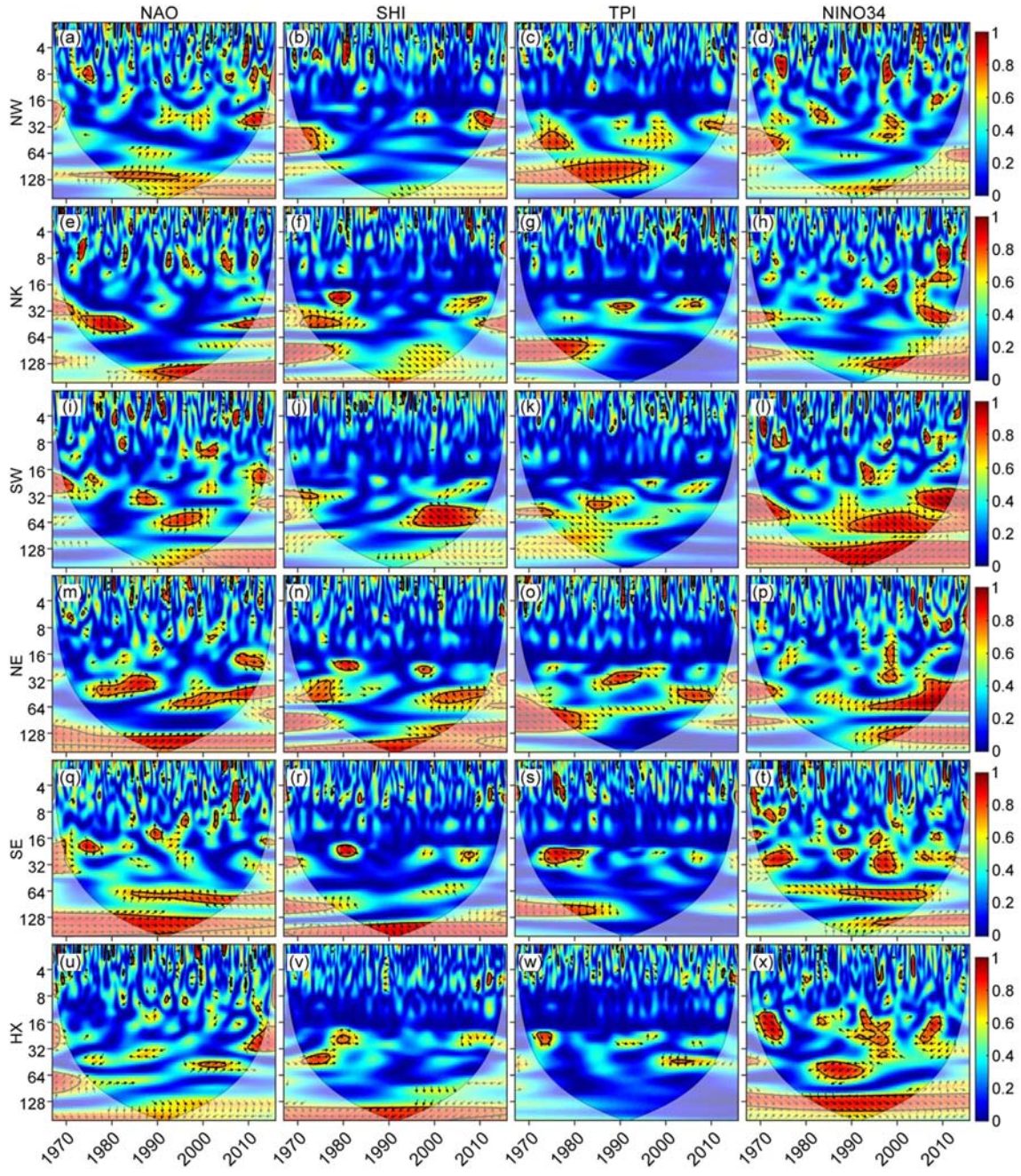

Fig. 8. Wavelet Coherence (WCO) between climate indices and spatially averaged SPEI12 for six sub-regions. The colors from blue to red indicate the increasing coherence. The solid black contours represent the significance of local power relative to the noise at a 0.05 level. The lighter shade area depicts the cone of influence (COI). The black arrows indicate the phase condition. The phase relationships between the climate indices and SPEI12 are denoted by arrows for in-phase pointing right, anti-phase pointing left; climate indices leading SPEI12 by 90° pointing up and SPEI leading climate indices by 90° pointing down. (For interpretation of the references to color in this figure legend, the reader is referred to the web version of this article.)

band during 2004–2015. Of special note is that a statistically significant coherence is detected during the whole study period at decadal scale (128–256 months) though the period before 1980 and after 2005 is possibly affected by the edge effect. SHI exhibits a significant coherence between 1996 and 2011 at 40–76 months scale.

For NE, the drought variation seems to be influenced by all four selected climate indices (NAO, SHI, TPI, and NINO34) in the band of 16–64 months. For example, there are strong correlations between NAO and SPEI for the 15–28 months band within the period from 2007 to 2013, the 28–48 months cycle during the period 1976–1990 and the 40–50 months band between 1993 and 2013. Similar significant patterns of SHI are also detected within 20–28 months cycle during 1978–1984 and 1997–2000 and within 40–64 months cycle during 1970–1978 and 2000–2011. TPI also exhibits obvious influence on drought variation with a strong coherence in 25–64 months during 1986–1995 and 2003–2010. A continuous significant coherence is found in the period of 1995–2013 at the scale of 32–64 months between NINO and SPEI. In addition, NAO and SHI display a significant coherence during the whole study period at the decadal scale (128–256 months) with SPEI leading phase.

The wavelet coherence at interannual scale (<80 months) in SE suggests that the drought variation is mainly related to NAO and NINO34. The identifiable coherence at 64–100 months scale is consistently detected after 1990. Similarly, the significant coherence patterns of

NINO34 with a large period amplitude (1–90 months) can also be observed in Fig. 8t. For instance, there are 1–32-month significant coherences during 1971–1977, 1987–1991 and 2006–2011; and a 64–90 months band coherence between 1987 and 2008. The significant coherence for time periods <90 months for SHI and TPI can only be detected within the time before 1990, which may indicate the weakening effect from both SH and TP. For the decadal scale, in-phase coherence during the whole study period is found for NAO.

NINO34 is the most influential climate index on the drought variation in the HX sub-region at the scale of 8–100 months. A lot of significant patterns are found for the 12–32 months band in the following periods: 1970–1975, 1992–1998 and 2005–2010. There is also a 48–80 month band detected during the period from 1982–1992. For the decadal scale (100–256 months), the in-phase and anti-phase relationship with drought variation marks the whole study period for NINO34 and SHI, though the period before 1980 and after 2000 is affected by the potential edge effect.

In general, the significant coherences between climate indices and drought variations in various sub-regions are quite different from each other. NINO34 shows significant correlations with *SPE*I in all six sub-regions. The effect from NAO is relatively smaller in the HX region than in the other sub-regions. SHI exhibits influence on drought variation in the eastern part of Central Asia (NE, SE, and HX) at the decadal scale. Compared with other climate indices, TPI has the smallest effect on drought variations over different sub-regions, although significant coherences are detected at the interannual scale (16–64 months) over NW, NE, and SE.

4. Discussion

Drought is a connection of several spheres including the atmosphere, hydrosphere, biosphere and anthroposphere. The effects of droughts are extensive and can involve various aspects such as water resources, agriculture, animal husbandry, environmental ecosystem, public health and so on.

Droughts have great impacts on local hydrological cycle. The headwater of rivers is sensitive to droughts with less human activities (Di Matteo et al., 2012; Di Matteo et al., 2017). During a drought period, high temperature may change the snow/ice melting time and the less precipitation in mountain region will decrease the accumulation of snow in headwater regions (Small et al., 2003). Provided a long enough duration, the precipitation deficit and high temperature may lead to soil dryness with negative effects on crops growth and livestock health, then increase the water demands for irrigation and exacerbate the already existing water crisis. Furtherly, the river flow and water storage of lakes drop. Besides the reduction of river flow, extended drought events may also lead to a reduction in groundwater level with negative effects on agriculture and water supply for industry and domestic sectors (Miyan, 2015). Without sufficient water supply, the environmental ecosystem of downstream and terminal lakes would be greatly affected because the semi-arid and arid ecosystem is highly dependent on the river (Li et al., 2015). The desiccation of Aral Sea is believed to be resulting from both inflow diversion for irrigation and reduced precipitation (Qi and Kulmatov, 2008). In this study, it is found that the Aral Sea region suffered from consistent drying trend and experienced more drought events with longer duration and larger severity. During drought periods, the Amu Darya River and the Syr Darya River provide less water flowing into the Aral Sea than the normal year as more water is extracted for irrigation and industry. For example, influenced by the drought during 2000–2002, the river flow dropped by 35% to 40% of the normal flow and the total inflow into the Aral Sea only amounted to 2 km^3/year (Micklin, 2016; Patrick, 2017). In turn, the desiccation of the Aral Sea had a significant impact on local climate and ecosystem resulting in an increment of drought days which may be as high as 300% (Glazovsky, 1995; Issanova and Abuduwaili, 2017b). It should be noted that a longer averaged drought duration and larger drought severity (Fig. 5) as well as a drying trend with larger magnitude (Fig. 6), are detected during the last 13 years (2003–2015) which should be paid enough attention by policy developers to avoid more negative effects such as serious forms of rapid soil and land degradation, water resources deficit, public health problems and great economic loss (Issanova and Abuduwaili, 2017a).

The agricultural damage induced by droughts is considerable in Central Asia. The damage to traditional rainfed agricultural areas and pasturelands is high due to soil moisture stress. For example, in Turkmenistan, the productivity of pasturelands are greatly reduced during drought periods. In a normal year, 2 ha of pasture can feed one sheep, while in the extremely dry years about 30 ha is required (Patrick, 2017). In addition, the large-scale irrigated croplands are also highly affected because of the scarce water resources. It is reported that harvests on rainfed and irrigated lands in a drought year can be reduced by 40% and 30%, which inevitably affects the food security of the population (Dahlstrom, 2012). In the 2000–2001 drought years, the direct agriculture loss reached up to 800 million dollars which is 5% GDP of Tajikistan (Patrick, 2017). All subregions except the NK sub-region experienced considerable drying trend since 2003. The drying trend in the last decade was also detected by Z. Li et al. (2017) based on PDSI drought index. In addition, the larger number of drought events occurred in summer over NK, SE and HX (Fig. 5). Due to large-scale and concentrated farmlands and grasslands and the fragile ecosystem in northwestern China (i.e. NE, SE and HX), the crop yields, animal husbandry and the local environmental ecosystem will be affected by the recent drying trend and the increasing short-term drought occurrence (Sataer, 2015). While the drought condition of the northern Kazakhstan seems to be better, where appears a consistent wetting trend from 1966 to 2015. This wetting trend may alleviate the local drought risk. However, it is found that this region experienced more short-term drought occurrences with higher intensity than the other regions, which is not good for the vegetation health, especially for the rainfed croplands and pastures (Issanova and Abuduwaili, 2017a).

Droughts may lead to a series of environmental problems. In arid and semi-arid regions, the land surface is covered by loose and fine materials. Therefore, the droughts and strong wind can easily lead to frequent dust and sandstorm (Indoitu et al., 2012). Without sufficient water to leach salts, the soil salinization is also a drought-induced environmental problem (Qi and Kulmatov, 2008). Moreover, a lot of social and economic issues are also related to droughts, including food security, environmental refugees, malnutrition and water-related diseases and so on. The results of this study, such as the spatiotemporal drought characteristics, drought trend, periodicity and links with large-scale climatic patterns are useful to understand the drought structure at a sub-regional scale and provide scientific basis for the mitigation of various drought impacts.

5. Conclusions

The understanding of the spatial and temporal variation of drought characteristics is vital for water resources management and drought mitigation. Based on long-term CRU dataset and multiscalar *SPE*I (i.e. SPEI3, SPEI6 and SPEI12), a series of drought characteristics including drought duration, frequency, severity, intensity, peak value and starting season are comprehensively investigated during 1966–2015 in this paper. The PCA and Varimax rotation technique are used for regionalization. The drought events and drought characteristics are analyzed based on the Run theory; the drought trend is detected by using the Sen's slope and the MMK method. Finally, the drought periodicity and the possible links between drought variation and large-scale climate patterns are investigated based on the wavelet analysis. The main results are summarized as follows.

(1) Based on the PCA and Varimax rotation method, Central Asia is divided into six sub-regions with different temporal drought

variations which include the northwest (NW), the north Kazakhstan (NK), the southwest (SW), the northeast (NE), the southeast (SE) and the Hexi Corridor region (HX).

(2) Three periods are found with the most severe drought events during the last half-century which are the 1973–1979 for the sub-regions of NW, NK, SW and SE; 1983–1988 for the sub-regions of SE and HX and the 1997–2003 for NE, NK, SW, SE and HX.

(3) The patterns of drought characteristics vary considerably in Central Asia. Specifically, the HX and the eastern part of SE are characterized by higher drought duration with lower drought intensity and severity. While NE experienced relatively fewer drought events with longer duration and severity, drought events over HX, SE, and part of NK seem to frequently occur in summer.

(4) Compared to 1966–2002, most parts of Central Asia (i.e. NW, SW, NK, NE, and northern SE) experienced a wet period characterized by lower drought frequency, shorter drought duration, lower drought severity and intensity in the latest 13 years. Exceptionally, the NW, HX and the eastern part of SE experienced more drought events at the 3-month timescale. Moreover, the Aral Sea region (central part of SW) suffered from longer drought duration and higher drought severity during 2003–2015.

(5) There is an overall wetting trend over Central Asia from 1966 to 2015 which results from both the drying trend over the central part of SW, the eastern part of SE and western HX and the wetting trend over the other regions. Except for NK, the other sub-regions show a significant drying trend during the period of 2003–2015. A continuously significant wetting trend is detected in NK during 1966–2015 while a slight and continuous drying trend occurred in HX.

(6) A common significant 16–64-month periodical oscillation can be detected in the *SPE*I series over the six sub-regions.

(7) Based on the cross-wavelet coherence, ENSO has an influence on drought variation over the whole region of Central Asia; NAO has significant coherence over all sub-regions except HX; SH exhibits influence over the eastern part of Central Asia and TP seems to have fewer effects on drought variation.

The results of this study may serve as scientific basis for policy design in the framework of water resources management and agricultural planning and may provide some reference to reduce the society and ecological influences over the arid lands of Central Asia at a sub-regional scale. For example, the drying trend in all sub-regions except the north Kazakhstan since 2003 and the increased drought duration and severity over the Aral Sea region could draw the attention of decision makers. The regional drying trend may lead to an increased societal and environmental vulnerability to droughts. The six sub-regions should be separately considered in the drought risk management. In addition, the related drought characteristics and climatic influences should be included in regional drought modeling and prediction. In future, the drought trend at both seasonal and annual scales and their impacts on vegetation ecosystems of Central Asia will be studied.

Acknowledgments

This work was jointly funded by the International Partnership Program ofthe Chinese Academy of Sciences under Grant No. 131551KYSB20160002, Tianshan Innovation Team Project of Xinjiang Department of Science and Technology (Grant No. Y744261), the Special Institute Main Service Program of the Chinese Academy of Sciences under Grant No. TSS-2015-014-FW-1-1 and the Key Laboratory Program of Xinjiang (No. 2015KL003). H.G. was supported by grants from the China Scholarship Council (201604910968) and the BOF co-funding from Ghent University (01SC5017) during his stay in Ghent University, Ghent, Belgium.

Appendix A. Supplementary data

Supplementary data to this article can be found online at https://doi.org/10.1016/j.scitotenv.2017.12.120.

References

Al-Kaisi, M.M., Elmore, R.W., Guzman, J.G., Hanna, H.M., Hart, C.E., Helmers, M.J., et al., 2013. Drought impact on crop production and the soil environment: 2012 experiences from Iowa. J. Soil Water Conserv. 68:19A–24A. https://doi.org/10.2489/jswc.68.1.19A.

Allen, R.G., Pereira, L.S., Raes, D., Smith, M., 1998. Crop Evapotranspiration-Guidelines for Computing Crop Water Requirements-FAO Irrigation and Drainage Paper 56. 300. FAO, Rome (D05109).

Andreadis, K.M., Clark, E.A., Wood, A.W., Hamlet, A.F., Lettenmaier, D.P., 2005. Twentieth-century drought in the conterminous United States. J. Hydrometeorol. 6:985–1001. https://doi.org/10.1175/Jhm450.1.

Ashraf, M., Routray, J.K., 2015. Spatio-temporal characteristics of precipitation and drought in Balochistan Province, Pakistan. Nat. Hazards 77:229–254. https://doi.org/10.1007/s11069-015-1593-1.

Bank, W., 2005. Drought: Management and Mitigation Assessment for Central Asia and the Caucasus. vol. 1 (Washington, DC).

Barlow, M., Cullen, H., Lyon, B., 2002. Drought in central and southwest Asia: La Nina, the warm pool, and Indian Ocean precipitation. J. Clim. 15:697–700. https://doi.org/10.1175/1520-0442(2002)015<0697:Dicasa>2.0.Co;2.

Bartlett, M.S., 1954. A note on the multiplying factors for various χ^2 approximations. J. R. Stat. Soc. Ser. B Methodol. 16, 296–298.

Bingyi, W., Jia, W., 2002. Possible impacts of winter Arctic Oscillation on Siberian high, the East Asian winter monsoon and sea-ice extent. Adv. Atmos. Sci. 19:297–320. https://doi.org/10.1007/s00376-002-0024-x.

Bond, N.R., Lake, P., Arthington, A.H., 2008. The impacts of drought on freshwater ecosystems: an Australian perspective. Hydrobiologia 600:3–16. https://doi.org/10.1007/s10750-008-9326-z.

Burroughs, W., 2003. Climate: Into the 21st Century. Cambridge University Press.

Cattell, R.B., 1966. The scree test for the number of factors. Multivar. Behav. Res. 1:245–276. https://doi.org/10.1207/s15327906mbr0102_10.

Chen, H., Sun, J., 2015. Changes in drought characteristics over China using the standardized precipitation evapotranspiration index. J. Clim. 28:5430–5447. https://doi.org/10.1175/Jcli-D-14-00707.1.

Cheng, C.-H., Nnadi, F., Liou, Y.-A., 2015. A regional land use drought index for Florida. Remote Sens. 7:17149–17167. https://doi.org/10.3390/rs71215879.

Cohen, J., Saito, K., Entekhabi, D., 2001. The role of the Siberian high in Northern Hemisphere climate variability. Geophys. Res. Lett. 28:299–302. https://doi.org/10.1029/2000gl011927.

Da Silva, R.M., Santos, C.A., Moreira, M., Corte-Real, J., Silva, V.C., Medeiros, I.C., 2015. Rainfall and river flow trends using Mann–Kendall and Sen's slope estimator statistical tests in the Cobres River basin. Nat. Hazards 77:1205–1221. https://doi.org/10.1007/s11069-015-1644-7.

Dahlstrom, R., 2012. Desert Problems and Desertification in Central Asia. Springer, Berlin; London.

Daufresne, M., Lengfellner, K., Sommer, U., 2009. Global warming benefits the small in aquatic ecosystems. Proc. Natl. Acad. Sci. U. S. A. 106:12788–12793. https://doi.org/10.1073/pnas.0902080106.

Deng, H., Chen, Y., 2017. Influences of recent climate change and human activities on water storage variations in Central Asia. J. Hydrol. 544:46–57. https://doi.org/10.1016/j.jhydrol.2016.11.006.

Di Lena, B., Vergni, L., Antenucci, F., Todisco, F., Mannocchi, F., 2013. Analysis of drought in the region of Abruzzo (Central Italy) by the standardized precipitation index. Theor. Appl. Climatol. 115:41–52. https://doi.org/10.1007/s00704-013-0876-2.

Di Matteo, L., Valigi, D., Cambi, C., 2012. Climatic characterization and response of water resources to climate change in limestone areas: considerations on the importance of geological setting. J. Hydrol. Eng. 18, 773–779.

Di Matteo, L., Dragoni, W., Maccari, D., Piacentini, S.M., 2017. Climate change, water supply and environmental problems of headwaters: the paradigmatic case of the Tiber, Savio and Marecchia rivers (Central Italy). Sci. Total Environ. 598:733–748. https://doi.org/10.1016/j.scitotenv.2017.04.153.

Dijk, A.I., Beck, H.E., Crosbie, R.S., Jeu, R.A., Liu, Y.Y., Podger, G.M., et al., 2013. The millennium drought in southeast Australia (2001–2009): natural and human causes and implications for water resources, ecosystems, economy, and society. Water Resour. Res. 49:1040–1057. https://doi.org/10.1002/wrcr.20123.

Ding, Y., Hayes, M.J., Widhalm, M., 2011. Measuring economic impacts of drought: a review and discussion. Disaster Prev. Manage. 20:434–446. https://doi.org/10.1108/09653561111161752.

Duan, A.M., Wu, G.X., 2005. Role of the Tibetan Plateau thermal forcing in the summer climate patterns over subtropical Asia. Clim. Dynam. 24:793–807. https://doi.org/10.1007/s00382-004-0488-8.

Gao, X., Zhao, Q., Zhao, X., Wu, P., Pan, W., Gao, X., et al., 2017. Temporal and spatial evolution of the standardized precipitation evapotranspiration index (SPEI) in the Loess Plateau under climate change from 2001 to 2050. Sci. Total Environ. 595:191–200. https://doi.org/10.1016/j.scitotenv.2017.03.226.

Gaybullaev, B., Chen, S.C., Kuo, Y.M., 2012. Large-scale desiccation of the Aral Sea due to over-exploitation after 1960. J. Mt. Sci. 9:538–546. https://doi.org/10.1007/s11629-012-2273-1.

Gibbs, W.J., 1967. Rainfall Deciles as Drought Indicators. vol. 33. Bureau of Meteorology Bull., Commonwealth of Australia, Melbourne, Australia, p. 48.

Glazovsky, N.F., 1995. The Aral Sea Basin. Springer Berlin Heidelberg, Berlin, Heidelberg.
Gong, D.Y., Ho, C.H., 2002. The Siberian High and climate change over middle to high latitude Asia. Theor. Appl. Climatol. 72:1–9. https://doi.org/10.1007/s007040200008.
Gregor, M., 2012. Surface and Groundwater Quality Changes in Periods of Water Scarcity. Springer Science & Business Media, Berlin Heidelberg.
Grinsted, A., Moore, J.C., Jevrejeva, S., 2004. Application of the cross wavelet transform and wavelet coherence to geophysical time series. Nonlinear Process Geophys. 11: 561–566. https://doi.org/10.5194/npg-11-561-2004.
Groll, M., Opp, C., Aslanov, I., 2013. Spatial and temporal distribution of the dust deposition in Central Asia – results from a long term monitoring program. Aeolian Res. 9: 49–62. https://doi.org/10.1016/j.aeolia.2012.08.002.
Guo, H., Chen, S., Bao, A.M., Hu, J.J., Gebregiorgis, A.S., Xue, X.W., et al., 2015. Intercomparison of high-resolution satellite precipitation products over Central Asia. Remote Sens. 7:7181–7211. https://doi.org/10.3390/rs70607181.
Guo, H., Bao, A.M., Liu, T., Chen, S., Ndayisaba, F., 2016. Evaluation of PERSIANN-CDR for meteorological drought monitoring over China. Remote Sens. 8:379. https://doi.org/10.3390/rs8050379.
Guo, H., Bao, A.M., Liu, T., Ndayisaba, F., He, D.M., Kurban, A., et al., 2017a. Meteorological drought analysis in the lower Mekong Basin using satellite-based long-term CHIRPS product. Sustainability 9:901. https://doi.org/10.3390/su9060901.
Guo, H., Bao, A.M., Ndayisaba, F., Liu, T., Kurban, A., De Maeyer, P., 2017b. Systematical evaluation of satellite precipitation estimates over Central Asia using an improved error-component procedure. J. Geophys. Res. 122:1–22. https://doi.org/10.1002/2017jd026877.
Hamed, K.H., Rao, A.R., 1998. A modified Mann-Kendall trend test for autocorrelated data. J. Hydrol. 204:182–196. https://doi.org/10.1016/S0022-1694(97)00125-X.
Heim, R.R., 2002. A review of twentieth-century drought indices used in the United States. Bull. Am. Meteorol. Soc. 83:1149–1165. https://doi.org/10.1175/1520-0477(2002)083<1149:AROTDI>2.3.CO;2.
Hoerling, M., Kumar, A., 2003. The perfect ocean for drought. Science 299:691–694. https://doi.org/10.1126/science.1079053.
Huang, J., Sun, S., Xue, Y., Li, J., Zhang, J., 2014. Spatial and temporal variability of precipitation and dryness/wetness during 1961–2008 in Sichuan Province, West China. Water Resour. Manage. 28:1655–1670. https://doi.org/10.1007/s11269-014-0572-8.
Huang, J., Xue, Y., Sun, S., Zhang, J., 2015. Spatial and temporal variability of drought during 1960–2012 in Inner Mongolia, north China. Quatern. Int. 355:134–144. https://doi.org/10.1016/j.quaint.2014.10.036.
Huang, S.Z., Huang, Q., Chang, J.X., Zhu, Y.L., Leng, G.Y., Xing, L., 2015. Drought structure based on a nonparametric multivariate standardized drought index across the Yellow River basin, China. J. Hydrol. 530:127–136. https://doi.org/10.1016/j.jhydrol.2015.09.042.
Huang, S.Z., Huang, Q., Leng, G.Y., Liu, S.Y., 2016. A nonparametric multivariate standardized drought index for characterizing socioeconomic drought: a case study in the Heihe River Basinx. J. Hydrol. 542:875–883. https://doi.org/10.1016/j.jhydro1.2016.09.059.
Huang, Q.Z., Zhang, Q., Singh, V.P., Shi, P.J., Zheng, Y.J., 2017. Variations of dryness/wetness across China: changing properties, drought risks, and causes. Global Planet. Change 155:1–12. https://doi.org/10.1016/j.gloplacha.2017.05.010.
Indoitu, R., Orlovsky, L., Orlovsky, N., 2012. Dust storms in Central Asia: spatial and temporal variations. J. Arid Environ. 85:62–70. https://doi.org/10.1016/j.jaridenv.2012.03.018.
Issanova, G., Abuduwaili, J., 2017a. Aeolian Processes in the Arid Territories of Central Asia. Springer.
Issanova, G., Abuduwaili, J., 2017b. Natural conditions of Central Asia and land-cover changes. Aeolian Processes in the Arid Territories of Central Asia and Kazakhstan. Springer, pp. 29–49.
Jensen, M.E., Burman, R.D., Allen, R.G., 1990. Evapotranspiration and irrigation water requirements. American Society for Civil Engineers. No. 70. ASCE, p. 360.
Jiang, L., Bao, A., Guo, H., Ndayisaba, F., 2017. Vegetation dynamics and responses to climate change and human activities in Central Asia. Sci. Total Environ. 599:967–980. https://doi.org/10.1016/j.scitotenv.2017.05.012.
Jones, P.D., Harpham, C., Harris, I., Goodess, C.M., Burton, A., Centella-Artola, A., et al., 2016. Long-term trends in precipitation and temperature across the Caribbean. Int. J. Climatol. 36:3314–3333. https://doi.org/10.1002/joc.4557.
Joshi, N., Gupta, D., Suryavanshi, S., Adamowski, J., Madramootoo, C.A., 2016. Analysis of trends and dominant periodicities in drought variables in India: a wavelet transform based approach. Atmos. Res. 182:200–220. https://doi.org/10.1016/j.atmosres.2016.07.030.
Kaiser, H.F., 1970. A second generation little jiffy. Psychometrika 35:401–415. https://doi.org/10.1007/BF02291817.
Kendall, M.G., 1990. Rank Correlation Methods. Charles Griffin, London.
Lee, S.-H., Yoo, S.-H., Choi, J.-Y., Bae, S., 2017. Assessment of the impact of climate change on drought characteristics in the Hwanghae Plain, North Korea using time series SPI and SPEI: 1981–2100. Water 9:579. https://doi.org/10.3390/w9080579.
Li, B., Su, H., Chen, F., Li, S., Tian, J., Qin, Y., et al., 2012. The changing pattern of droughts in the Lancang River Basin during 1960–2005. Theor. Appl. Climatol. 111:401–415. https://doi.org/10.1007/s00704-012-0658-2.
Li, Z., Chen, Y.N., Li, W.H., Deng, H.J., Fang, G.H., 2015. Potential impacts of climate change on vegetation dynamics in Central Asia. J. Geophys. Res. 120:12345–12356. https://doi.org/10.1002/2015jd023618.
Li, Z., Chen, Y.N., Wang, Y., Fang, G.H., 2016. Dynamic changes in terrestrial net primary production and their effects on evapotranspiration. Hydrol. Earth Syst. Sci. 20: 2169–2178. https://doi.org/10.5194/hess-20-2169-2016.
Li, Y., Chen, C., Sun, C., 2017. Drought severity and change in Xinjiang, China, over 1961–2013. Hydrol. Res. 48:1343–1362. https://doi.org/10.2166/nh.2016.026.
Li, Z., Chen, Y., Fang, G., Li, Y., 2017b. Multivariate assessment and attribution of droughts in Central Asia. Sci. Rep. 7:1316. https://doi.org/10.1038/s41598-017-01473-1.
Lioubimtseva, E., Cole, R., 2006. Uncertainties of climate change in arid environments of Central Asia. Rev. Fish. Sci. 14:29–49. https://doi.org/10.1080/10641260500340603.
Lioubimtseva, E., Henebry, G.M., 2009. Climate and environmental change in arid Central Asia: impacts, vulnerability, and adaptations. J. Arid Environ. 73:963–977. https://doi.org/10.1016/j.jaridenv.2009.04.022.
Lioubimtseva, E., Cole, R., Adams, J.M., Kapustin, G., 2005. Impacts of climate and land-cover changes in arid lands of Central Asia. J. Arid Environ. 62:285–308. https://doi.org/10.1016/j.jaridenv.2004.11.005.
Liu, Z., Zhou, P., Zhang, F., Liu, X., Chen, G., 2013. Spatiotemporal characteristics of dryness/wetness conditions across Qinghai Province. Northwest China. Agr. Forest Meteorol. 182:101–108. https://doi.org/10.1016/j.agrformet.2013.05.013.
Liu, X., Wang, S., Zhou, Y., Wang, F., Li, W., Liu, W., 2015. Regionalization and spatiotemporal variation of drought in China based on standardized precipitation evapotranspiration index (1961–2013). Adv. Meteorol. 2015:1–18. https://doi.org/10.1155/2015/950262.
Liu, Z., Wang, Y., Shao, M., Jia, X., Li, X., 2016. Spatiotemporal analysis of multiscalar drought characteristics across the Loess Plateau of China. J. Hydrol. 534:281–299. https://doi.org/10.1016/j.jhydrol.2016.01.003.
Liu, Y., Zhu, Y., Ren, L., Singh, V.P., Yang, X., Yuan, F., 2017. A multiscalar Palmer drought severity index. Geophys. Res. Lett. 44:6850–6858. https://doi.org/10.1002/2017GL073871.
Lubin, N., 2016. Labour and Nationality in Soviet Central Asia: An Uneasy Compromise. Springer, Basingstoke.
Mallya, G., Mishra, V., Niyogi, D., Tripathi, S., Govindaraju, R.S., 2016. Trends and variability of droughts over the Indian monsoon region. Weather Clim. Extrem. 12:43–68. https://doi.org/10.1016/j.wace.2016.01.002.
Mann, H.B., 1945. Nonparametric tests against trend. Econometrica 13:245–259. https://doi.org/10.2307/1907187.
Maraun, D., Kurths, J., 2004. Cross wavelet analysis: significance testing and pitfalls. Nonlinear Process Geophys. 11:505–514. https://doi.org/10.5194/npg-11-505-2004.
Mariotti, A., 2007. How ENSO impacts precipitation in southwest central Asia. Geophys. Res. Lett. 34, L16706. https://doi.org/10.1029/2007GL030078.
McKee, T.B., Doesken, N.J., Kleist, J., 1993. The Relationship of Drought Frequency and Duration to Time Scales. Eighth Conference on Applied Climatology, Anaheim, California, pp. 17–22.
Merino, A., Lopez, L., Hermida, L., Sanchez, J.L., Garcia-Ortega, E., Gascon, E., et al., 2015. Identification of drought phases in a 110-year record from Western Mediterranean basin: trends, anomalies and periodicity analysis for Iberian Peninsula. Global Planet. Change 133:96–108. https://doi.org/10.1016/j.gloplacha.2015.08.007.
Micklin, P., 2016. The future Aral Sea: hope and despair. Environ. Earth Sci. 75:1–15. https://doi.org/10.1007/s12665-016-5614-5.
Mishra, A.K., Singh, V.P., 2010. A review of drought concepts. J. Hydrol. 391:204–216. https://doi.org/10.1016/j.jhydrol.2010.07.012.
Mishra, A.K., Ines, A.V.M., Das, N.N., Khedun, C.P., Singh, V.P., Sivakumar, B., et al., 2015. Anatomy of a local-scale drought: application of assimilated remote sensing products, crop model, and statistical methods to an agricultural drought study. J. Hydrol. 526: 15–29. https://doi.org/10.1016/j.jhydrol.2014.10.038.
Mitchell, T.D., Jones, P.D., 2005. An improved method of constructing a database of monthly climate observations and associated high-resolution grids. Int. J. Climatol. 25:693–712. https://doi.org/10.1002/joc.1181.
Mitchell Jr., J., Dzerdzeevskii, B., Flohn, H., Hofmeyr, W., Lamb, H., Rao, K., et al., 1966. Climatic change. WMO Technical Note, 79 (WMO-No. 195/TP. 100). World Meteorological Organization, Geneva, p. 79.
Miyan, M.A., 2015. Droughts in Asian least developed countries: vulnerability and sustainability. Weather Clim. Extrem. 7:8–23. https://doi.org/10.1016/j.wace.2014.06.003.
Mo, K.C., 2011. Drought onset and recovery over the United States. J. Geophys. Res. 116: 1–14. https://doi.org/10.1029/2011jd016168.
Montaseri, M., Amirataee, B., 2017. Comprehensive stochastic assessment of meteorological drought indices. Int. J. Climatol. 37:998–1013. https://doi.org/10.1002/joc.4755.
Mughal, M.A.Z., 2013. Pamir Alpine desert and tundra. Biomes Ecosyst. 3, 978–980.
Nam, W.H., Choi, J.Y., Yoo, S.H., Jang, M.W., 2012. A decision support system for agricultural drought management using risk assessment. Paddy Water Environ. 10:197–207. https://doi.org/10.1007/s10333-012-0329-z.
North, G.R., Bell, T.L., Cahalan, R.F., Moeng, F.J., 1982. Sampling errors in the estimation of empirical orthogonal functions. Mon. Weather Rev. 110:699–706. https://doi.org/10.1175/1520-0493(1982)110<0699:Seiteo>2.0.Co;2.
Palmer, W.C., 1965. Meteorological Drought. vol. 30. US Department of Commerce, Weather Bureau Washington, DC, USA, U.S.
Palmer, W.C., 1968. Keeping track of crop moisture conditions, nationwide: the new crop moisture index. Weatherwise 21:156–161. https://doi.org/10.1080/00431672.1968.9932814.
Panagiotopoulos, F., Shahgedanova, M., Hannachi, A., Stephenson, D.B., 2005. Observed trends and teleconnections of the Siberian high: a recently declining center of action. J. Clim. 18:1411–1422. https://doi.org/10.1175/Jcli3352.1.
Patrick, E., 2017. Drought characteristics and management in Central Asia and Turkey. FAO Water Reports. FAO, p. 114.
Paulo, A., Rosa, R., Pereira, L., 2012. Climate trends and behaviour of drought indices based on precipitation and evapotranspiration in Portugal. Nat. Hazards Earth Syst. Sci. 12: 1481–1491. https://doi.org/10.5194/nhess-12-1481-2012.
Portela, M.M., dos Santos, J.F., Silva, A.T., Benitez, J.B., Frank, C., Reichert, J.M., 2015. Drought analysis in southern Paraguay, Brazil and northern Argentina: regionalization, occurrence rate and rainfall thresholds. Hydrol. Res. 46:792–810. https://doi.org/10.2166/nh.2014.074.
Portela, M.M., Zeleňáková, M., Santos, J.F., Purcz, P., Silva, A.T., Hlavatá, H., 2017. Comprehensive characterization of droughts in Slovakia. Int. Environ. Sci. Dev. 8:25–29. https://doi.org/10.18178/ijesd.2017.8.1.915.

Qi, J., Kulmatov, R., 2008. An overview of environmental issues in Central Asia. Environmental Problems of Central Asia and Their Economic, Social and Security Impacts. Springer, pp. 3–14.
Qi, J.G., Bobushev, T.S., Kulmatov, R., Groisman, P., Gutman, G., 2012. Addressing global change challenges for Central Asian socio-ecosystems. Front. Earth Sci. 6:115–121. https://doi.org/10.1007/s11707-012-0320-4.
Rayner, N.A., Parker, D.E., Horton, E.B., Folland, C.K., Alexander, L.V., Rowell, D.P., et al., 2003. Global analyses of sea surface temperature, sea ice, and night marine air temperature since the late nineteenth century. J. Geophys. Res. 108:1–22. https://doi.org/10.1029/2002jd002670.
Raziei, T., Saghafian, B., Paulo, A.A., Pereira, L.S., Bordi, I., 2009. Spatial patterns and temporal variability of drought in Western Iran. Water Resour. Manage. 23:439–455. https://doi.org/10.1007/s11269-008-9282-4.
Raziei, T., Bordi, I., Pereira, L.S., 2012. Regional drought modes in Iran using the SPI: the effect of time scale and spatial resolution. Water Resour. Manage. 27:1661–1674. https://doi.org/10.1007/s11269-012-0120-3.
Richman, M.B., 1986. Rotation of principal components. J. Climatol. 6:293–335. https://doi.org/10.1002/joc.3370060305.
Sataer, G., 2015. Spatial Patterns of Drought Persistence in Xinjiang (AR), China. Western Michigan University, p. 607.
Sen, P.K., 1968. Estimates of the regression coefficient based on Kendall's tau. J. Am. Stat. Assoc. 63:1379–1389. https://doi.org/10.2307/2285891.
Sheffield, J., Wood, E.F., 2007. Characteristics of global and regional drought, 1950–2000: analysis of soil moisture data from off-line simulation of the terrestrial hydrologic cycle. J. Geophys. Res. 112, D17115. https://doi.org/10.1029/2006JD008288.
Sheffield, J., Wood, E.F., 2008. Projected changes in drought occurrence under future global warming from multi-model, multi-scenario, IPCC AR4 simulations. Clim. Dynam. 31:79–105. https://doi.org/10.1007/s00382-007-0340-z.
Sheffield, J., Wood, E.F., 2012. Drought: Past Problems and Future Scenarios. Taylor and Francis, Hoboken.
Sheffield, J., Andreadis, K.M., Wood, E.F., Lettenmaier, D.P., 2009. Global and continental drought in the second half of the twentieth century: severity–area–duration analysis and temporal variability of large-scale events. J. Clim. 22:1962–1981. https://doi.org/10.1175/2008jcli2722.1.
Small, I., Falzon, D., Van Der Meer, J.B., Ford, N., 2003. Safe water for the Aral Sea Area: could it get any worse? Eur. J. Pub. Health 13, 87–89.
Spinoni, J., Naumann, G., Carrao, H., Barbosa, P., Vogt, J., 2014. World drought frequency, duration, and severity for 1951–2010. Int. J. Climatol. 34:2792–2804. https://doi.org/10.1002/joc.3875.
von Storch, H., Zwiers, F.W., 2002. Statistical Analysis in Climate Research. Cambridge University Press, Cambridge.
Suryavanshi, S., Pandey, A., Chaube, U., Joshi, N., 2014. Long-term historic changes in climatic variables of Betwa Basin, India. Theor. Appl. Climatol. 117:403–418. https://doi.org/10.1007/s00704-013-1013-y.
Svoboda, M., Hayes, M., Wood, D., 2012. Standardized precipitation index user guide. In: Svoboda MHaDW, M. (Ed.), Technical Report WMO-No. 1090. World Meteorological Organization (WMO), Geneva, p. 24.
Tabari, H., Talaee, P.H., Nadoushani, S.S.M., Willems, P., Marchetto, A., 2014. A survey of temperature and precipitation based aridity indices in Iran. Quatern. Int. 345: 158–166. https://doi.org/10.1016/j.quaint.2014.03.061.
Telesca, L., Vicente-Serrano, S.M., Lopez-Moreno, J.I., 2013. Power spectral characteristics of drought indices in the Ebro river basin at different temporal scales. Stoch. Env. Res. Risk A 27:1155–1170. https://doi.org/10.1007/s00477-012-0651-4.
Thavorntam, W., Tantemsapya, N., Armstrong, L., 2015. A combination of meteorological and satellite-based drought indices in a better drought assessment and forecasting in Northeast Thailand. Nat. Hazards 77:1453–1474. https://doi.org/10.1007/s11069-014-1501-0.
Thornthwaite, C.W., 1948. An approach toward a rational classification of climate. Geog. Rev. 38:55–94. https://doi.org/10.2307/210739.
Torrence, C., Compo, G.P., 1998. A practical guide to wavelet analysis. Bull. Am. Meteorol. Soc. 79:61–78. https://doi.org/10.1175/1520-0477(1998)079<0061:Apgtwa>2.0.Co;2.
Venturas, M.D., MacKinnon, E.D., Dario, H.L., Jacobsen, A.L., Pratt, R.B., Davis, S.D., 2016. Chaparral shrub hydraulic traits, size, and life history types relate to species mortality during California's historic drought of 2014. PLoS One 11, e0159145. https://doi.org/10.1371/journal.pone.0159145.
Vicente-Serrano, S.M., Lopez-Moreno, J.I., 2005. Hydrological response to different time scales of climatological drought: an evaluation of the standardized precipitation index in a mountainous Mediterranean basin. Hydrol. Earth Syst. Sci. 9:523–533. https://doi.org/10.5194/hess-9-523-2005.
Vicente-Serrano, S.M., Begueria, S., Lopez-Moreno, J.I., 2010. A multiscalar drought index sensitive to global warming: the standardized precipitation evapotranspiration index. J. Clim. 23:1696–1718. https://doi.org/10.1175/2009jcli2909.1.
Vu, M.T., Raghavan, S.V., Pham, D.M., Liong, S.-Y., 2015. Investigating drought over the Central Highland, Vietnam, using regional climate models. J. Hydrol. 526:265–273. https://doi.org/10.1016/j.jhydrol.2014.11.006.
Wang, Q., Wu, J., Lei, T., He, B., Wu, Z., Liu, M., et al., 2014. Temporal-spatial characteristics of severe drought events and their impact on agriculture on a global scale. Quatern. Int. 349:10–21. https://doi.org/10.1016/j.quaint.2014.06.021.
Wang, H.J., Chen, Y.N., Li, W.H., 2015a. Characteristics in streamflow and extremes in the Tarim River, China: trends, distribution and climate linkage. Int. J. Climatol. 35: 761–776. https://doi.org/10.1002/joc.4020.
Wang, H.J., Chen, Y.N., Pan, Y.P., Li, W.H., 2015b. Spatial and temporal variability of drought in the arid region of China and its relationships to teleconnection indices. J. Hydrol. 523:283–296. https://doi.org/10.1016/j.jhydrol.2015.01.055.
Wang, Q., Shi, P., Lei, T., Geng, G., Liu, J., Mo, X., et al., 2015. The alleviating trend of drought in the Huang-Huai-Hai Plain of China based on the daily SPEI. Int. J. Climatol. 35: 3760–3769. https://doi.org/10.1002/joc.4244.
Wang, Y., Zhang, T., Chen, X., Li, J., Feng, P., 2017. Spatial and temporal characteristics of droughts in Luanhe River basin, China. Theor. Appl. Climatol. 2017:1–17. https://doi.org/10.1007/s00704-017-2059-z.
Wang, Z., Li, J., Lai, C., Huang, Z., Zhong, R., Zeng, Z., et al., 2017b. Increasing drought has been observed by SPEI_pm in Southwest China during 1962–2012. Theor. Appl. Climatol.:1–16 https://doi.org/10.1007/s00704-017-2152-3.
Wells, N., Goddard, S., Hayes, M.J., 2004. A self-calibrating Palmer drought severity index. J. Clim. 17:2335–2351. https://doi.org/10.1175/1520-0442(2004)017<2335:Aspdsi>2.0.Co;2.
Wilhite, D.A., 1996. A methodology for drought preparedness. Nat. Hazards 13, 229–252.
Wu, H., Wilhite, D.A., 2004. An operational agricultural drought risk assessment model for Nebraska, USA. Nat. Hazards 33:1–21. https://doi.org/10.1023/B:Nhaz.0000034994.44357.75.
Wu, H., Hayes, M.J., Weiss, A., Hu, Q., 2001. An evaluation of the standardized precipitation index, the China-Z index and the statistical Z-score. Int. J. Climatol. 21:745–758. https://doi.org/10.1002/joc.658.
Xu, H.J., Wang, X.P., Zhang, X.X., 2016. Decreased vegetation growth in response to summer drought in Central Asia from 2000 to 2012. Int. J. Appl. Earth Obs. 52:390–402. https://doi.org/10.1016/j.jag.2016.07.010.
Xu, B., Yang, Q., Ma, Z., 2017. Decadal characteristics of global land annual precipitation variation on multiple spatial scales. Chinese J. Atmos. Sci. 41:593–602. https://doi.org/10.3878/j.issn.1006-9895.1608.16174.
Yang, H., Yang, D., Hu, Q., Lv, H., 2014. Spatial variability of the trends in climatic variables across China during 1961–2010. Theor. Appl. Climatol. 120:773–783. https://doi.org/10.1007/s00704-014-1208-x.
Yevjevich, V.M., 1967. An Objective Approach to Definition and Investigations of Continental Hydrologic Droughts. vol. 23. Colorado State University, Fort Collins, Colorado.
Yin, G., Hu, Z., Chen, X., Tiyip, T., 2016. Vegetation dynamics and its response to climate change in Central Asia. J. Arid Land. 8:375–388. https://doi.org/10.1007/s40333-016-0043-6.
Yoon, J.-H., Mo, K., Wood, E.F., 2012. Dynamic-model-based seasonal prediction of meteorological drought over the contiguous United States. J. Hydrometeorol. 13:463–482. https://doi.org/10.1175/Jhm-D-11-038.1.
Yu, X., Zhao, G., Zhao, W., Yan, T., Yuan, X., 2017. Analysis of precipitation and drought data in Hexi Corridor, Northwest China. Hydrology 4:29. https://doi.org/10.3390/hydrology4020029.
Zeleke, T., Giorgi, F., Diro, G., Zaitchik, B., 2017. Trend and periodicity of drought over Ethiopia. Int. J. Climatol. 37, 4733–4748.
Zhang, Q., Li, J.F., Singh, V.P., Bai, Y.G., 2012. SPI-based evaluation of drought events in Xinjiang, China. Nat. Hazards 64:481–492. https://doi.org/10.1007/s11069-012-0251-0.
Zhang, Z., Chen, X., Xu, C.-Y., Hong, Y., Hardy, J., Sun, Z., 2015. Examining the influence of river–lake interaction on the drought and water resources in the Poyang Lake basin. J. Hydrol. 522:510–521. https://doi.org/10.1016/j.jhydrol.2015.01.008.
Zhang, Q., Kong, D.D., Singh, V.P., Shi, P.J., 2017. Response of vegetation to different time-scales drought across China: spatiotemporal patterns, causes and implications. Global Planet. Change 152:1–11. https://doi.org/10.1016/j.gloplacha.2017.02.008.
Zhao, G.J., Mu, X.M., Hormann, G., Fohrer, N., Xiong, M., Su, B.D., et al., 2012. Spatial patterns and temporal variability of dryness/wetness in the Yangtze River Basin, China. Quatern. Int. 282:5–13. https://doi.org/10.1016/j.quaint.2011.10.020.
Zhao, X., Li, Z., Zhu, Q., Zhu, D., Liu, H., 2017. Climatic and drought characteristics in the loess hilly-gully region of China from 1957 to 2014. PLoS One 12, e0178701. https://doi.org/10.1371/journal.pone.0178701.
Zhu, Y., Chang, J., Huang, S., Huang, Q., 2016. Characteristics of integrated droughts based on a nonparametric standardized drought index in the Yellow River Basin, China. Hydrol. Res. 47:454–467. https://doi.org/10.2166/nh.2015.287.